Canopy interception mapping using field measurements and high-resolution airborne imagery

case study for a region in Vorarlberg, Austria

Universiteit Utrecht

P.C.Vermunt

March 2016

Canopy interception mapping using field measurements and high-resolution airborne imagery

case study for a region in Vorarlberg, Austria

MSc thesis
MSc programme: Earth Surface & Water
Track: Hydrology
Faculty of Geosciences
Department of Physical Geography
Utrecht University
Heidelberglaan 2
3584CS Utrecht

Author
Paul Vermunt
E-mail: p.c.vermunt@students.uu.nl
Student number: 3709035

Supervisors
Dr. L.P.H. van Beek
E-mail: R.vanBeek@uu.nl
Department of Physical Geography, Utrecht University

Prof. Dr. S.M. de Jong
E-mail: S.M.deJong@uu.nl
Department of Physical Geography, Utrecht University

Abstract

The process of rainfall interception by canopies plays an important role in the hydrological cycle. The fraction of rainfall which is intercepted is largely dependent on species-specific vegetation properties, such as leaf- and branch architecture and canopy structure and - density. Because these vegetation properties spatially vary, canopy interception is a spatially variable process. However, these species-specific vegetation properties are often not, or insufficiently included in hydrological models which focus for example on rainfall-runoff processes, soil moisture balances, transpiration and groundwater recharge from rainfall. This could lead to serious modelling uncertainties and - mistakes. This study aimed at improving an existing spatial interception mapping approach by including relations between species-specific vegetation properties and interception. In order to achieve this goal, a two-fold method was applied. First, the influence of species-specific differences of leaf-and canopy structures on the interception process was studied. Fieldwork on branch- and plot-scale was performed in a study region in Vorarlberg (Austria) to find relations between the vegetation properties and interception. Secondly, the ability of a high-resolution remote sensing imagery based model to estimate the spatial variability of canopy interception on regional scale was studied when these species-specific relations were implemented. Promising fieldwork results were gained which describe the relations between vegetation properties and interception per species. Due to these results, it was possible to model spatial variability of canopy interception for the study region in Vorarlberg, thereby taking species-specific vegetation properties into account. Although the results contribute to the improvement of the current approach to quantitatively estimate spatial variability of canopy interception on regional scale, the method needs to be improved and more research is needed in this field.

Keywords: Canopy interception; Spatial variability; Species-specific leaf -and canopy structure; Remote sensing; High-resolution data; Field measurements

Preface

This study was performed as part of the BioSLIDE project (The influence of **Bio**mass and its change on Land**SLIDE** activity), which is a collaborative project of the Department of Geography and Regional Research (University of Vienna), the Department of Geodesy and Geo-information (Vienna University of Technology), the Faculty of Geosciences (University of Utrecht) and the Faculty of Civil Engineering and Geosciences (University of Technology, Delft). The main objective of this project is to investigate, quantify and assess the spatial - and temporal hydrological and geomechanical effects of vegetation and vegetation changes on landslide triggering and activity. A physically based hydro-mechanical model is used to simulate both the effect of vegetation and its change and the influence of climatic variations on slope stability.

The MSc thesis represents an important part of the *Hydrology*-track programme of the master *Earth Surface and Water* at Utrecht University. The knowledge and skills which were gained from courses in the first year of the master's programme were used to perform this study. However, this would not have been possible without the efforts of some people, who should be thanked here.

Special thanks go to my supervisors Rens van Beek and Steven de Jong, who guided me through the process of research from the beginning to the end. I can truly say that I have learned a lot from the supervision during meetings and by e-mail. I would also like to thank my fieldwork partner Elmar Schmaltz, who supported me not only during fieldwork, but also helped me with the data collection and with all the contacts he has to provide me with information. Additionally, thanks to Maarten Zeylmans van Emmichoven, who helped me to deal with the difficulties in the dataset and GIS-software. Finally, my thanks also go to the other members of the Department of Physical Geography who were willing to answer my questions and helped me with some equipment and advice for the fieldwork campaign.

Utrecht, March 2016
Paul Vermunt

Content

1. Introduction

1.1 Background

The process of rainfall interception plays an important role in the hydrological cycle. Interception loss can generally be defined as the amount of rainfall which is caught and retained by vegetation or other surface covers and subsequently is evaporated back into the atmosphere (Merriam, 1960; Dunne & Leopold, 1978; Aston, 1979; Anzhi *et al*., 2005). The most studied form of interception is interception by forests, whereby a distinction can be made between canopy interception and interception by the forest floor litter (Dunne & Leopold, 1978). Canopy interception is related to the rainfall which is retained by the leaves and twigs, and leads to a spatial and temporal redistribution of rainfall to the ground or atmosphere (Merriam, 1960; Tromble, 1983). Rainfall which can not be retained by the leaves and twigs penetrates the canopy by stemflow and throughfall, which can either be directly through open spaces between the leaves, or indirectly by leaf drip. A portion of the throughfall and stemflow never reaches the soil, because it is stored in the forest floor litter or evaporates back into the atmosphere. The latter process is defined as forest floor interception (Dunne & Leopold, 1978; Anzhi, 2005; Gerrits, 2010).

Extensive research has been performed to determine the actual influence of canopies on the interception process. The fractions of precipitation intercepted by canopies range between 6 and 57% (Helvey & Patric, 1965; Swank, 1968; Lull & Sopper, 1969; Tromble, 1983; Liu, 1997; Crockford & Richardson, 2000; Savenije, 2004; Anzhi *et al*., 2005; Herbst *et al*., 2006; Gerrits, 2010; Gerrits *et al*., 2010). This large range can be explained by multiple factors, divided into two main sources. First, the proportion of precipitation intercepted by the canopy is dependent on spatial - and temporal climatic differences. Dry periods or dry areas for example have generally larger interception-precipitation ratios than humid periods or -areas, simply because the amount of rain that falls is small and therefore relatively more rainfall can be intercepted (Llorens *et al.*, 1997; Savenije, 2004; Gerrits *et al*., 2010). Second, spatial - and temporal differences in the density and structure of the foliage create differences in interception fractions. Temporal differences in foliage density can particularly be observed for deciduous trees, which lose their leaves during the transition from the growing to the dormant season. Hence, less leaves are present during the dormant season to intercept rain. In contrary, most coniferous trees have a more or less constant foliage throughout the year and therefore have a lower seasonal variability of interception (Sopper & Lull, 1969; Dunne & Leopold, 1978; Herbst *et al*., 2006; Gerrits, 2010). Furthermore, due to a variability of tree species and - ages, (natural) forests are extremely spatially diverse when it comes to canopy structures and - densities (Parker, 1995; Gould, 2000; Wirth et al., 2001; Leuzinger & Körner, 2007). For example, coniferous trees have generally higher leaf densities per projected area than broad-leaved trees (Parker, 1995). Besides, some species are characterised by strongly clumped foliage along branches and branch tips and/or clustered foliage rather than a homogeneous distribution of leaves (Parker, 1995). These structures influence the canopy closure and hence the interception surface. Furthermore, the horizontal - and vertical distribution and extent of leaves differ for tree ages and - species. Generally, older trees have developed leaves over a large range of heights (dependent on competition for light) than younger trees and have a broader horizontal extent. Therefore, the leaf density and canopy closure is generally higher for older trees (Parker, 1995). These structures and densities of the canopies partly determine the extent to which rain is intercepted. Besides, the building components of these canopies, the branches with leaves or needles, vary between species when it comes to (rain) water detention, due to different leaf - and

branch shape and texture (Herwitz, 1985; Parker, 1995; Llorens & Gallart, 2000; De Jong & Jetten, 2007).

In contrary to canopy interception, much less research is conducted on forest floor litter interception, and the existing research shows large variation in results. Helvey & Patric (1965) for example estimate an amount of 2 to 5% of the annual rainfall in the southern Appalachians to be intercepted by the forest floor litter. Gerrits (2010) however finds an annually constant forest floor litter interception for beech leaves - and Cedar needle floors of 22% and 18% respectively. Just as for canopy interception, these differences in interception fractions can be attributed to the number - and architecture of the leaves in the litter layer and the weather characteristics (Gerrits, 2010).

Because these canopy- and forest floor litter characteristics spatially and temporarily vary and largely influence the fraction of precipitation which ends up as interception loss, it is crucial to include these characteristics in spatio-temporal hydrological models which focus on rainfall-runoff processes, soil moisture balances, transpiration and groundwater recharge from rainfall. When the interception process is not adequately included in these models, this could lead to serious modelling uncertainties and - mistakes, especially when the error of incorrectly modelled interception is compensated by other parameters, to get the best fit (Savenije, 2004; Bulcock & Jewitt, 2010).

However, little research has been conducted on the species-specific relations between interception and plant properties such as leaf architecture and canopy structure. Consequently, these relations are often not, or insufficiently included in existing quantitative modelling methods of spatially varying interception losses. A promising approach to address the problem of spatial variability of tree characteristics in interception modelling was developed by De Jong & Jetten (2007). They developed a method to quantitatively estimate canopy interception using earth observation images or remote sensing. An extension of an existing exponential interception model (Merriam, 1960; Aston, 1979) was used to estimate the canopy interception per grid cell. This exponential model uses parameters which are based on vegetation characteristics such as leaf area index (LAI), canopy cover and maximum water detention. These parameters were derived from earth observation products, existing relations between these products and model parameters, and existing field relations between the different model parameters. However, although this method seems to be a promising approach to quantitatively estimate canopy interception on regional scales, it does not include a detailed description of species-specific leaf architecture and - canopy structure. Besides, the method is not tested with field measurements of canopy interception for different rainfall events.

1.2 Aim and objectives

This study focused on the spatial variability of canopy interception rather than forest floor interception. The study aimed at improving the spatial interception mapping approach described by De Jong & Jetten (2007) by using species-specific relations between vegetation properties and interception. The study area of this research project is a region of ~15 km^2 located in the federal state of Vorarlberg, Austria, which is selected by the BioSLIDE project because of the presence of (scars of) landslides in this area and the availability of high-resolution airborne remote sensing imagery. The required measurements were conducted within the borders of this study area during a three-week period of fieldwork. The following research objectives were attempted to be achieved: (1) study the influence of species-specific differences of leaf- and canopy structures on the interception process; (2) study the influence of these differences on the spatial variability of canopy interception on regional scale when implementing them into a high-resolution remote sensing imagery based model.

1.3 Thesis outline

After this introduction, the thesis starts with a literature overview of the relief, climate and vegetation of the study area (chapter 2). This chapter serves as background information for the reader to gain insight into the physical geographical processes which are important for canopy interception. Thereafter, the methodology is described in chapter 3. The methodology starts with an extensive description of the theoretical canopy interception model. Next, the methods of the model parameter calculations are divided into fieldwork methods and remote sensing image processing methods. The methodology chapter is followed by the results (chapter 4), which are divided into the fieldwork results, the image processing results and the final model results. The methodology and the results are extensively discussed in chapter 5. In the final chapter, chapter 6, it is discussed whether the research aim and objectives are reached and answers on the research questions are attempted to give. In the same chapter, recommendations for further research are given.

2. Research area

The study area is situated in the federal state of Vorarlberg, in the western part of Austria (figure 2.1) and has a size of ~15 km^2. This region was selected as study area for the BioSLIDE project for several reasons. The main criterion for the study area was the presence of several easily accessible landslides, which is the case for this region. Besides, very detailed data is available for this region, including high resolution ALS (airborne laser scanning) data, geologic information and multi-temporal aerial photographs (1950s-2012). The latter source of data is used in this study and will be described in the methodology (chapter 3). Furthermore, the area has a relatively homogeneous geology and is easy to reach due to a good infrastructure (E. Schmaltz, personal communication, February 9, 2016).

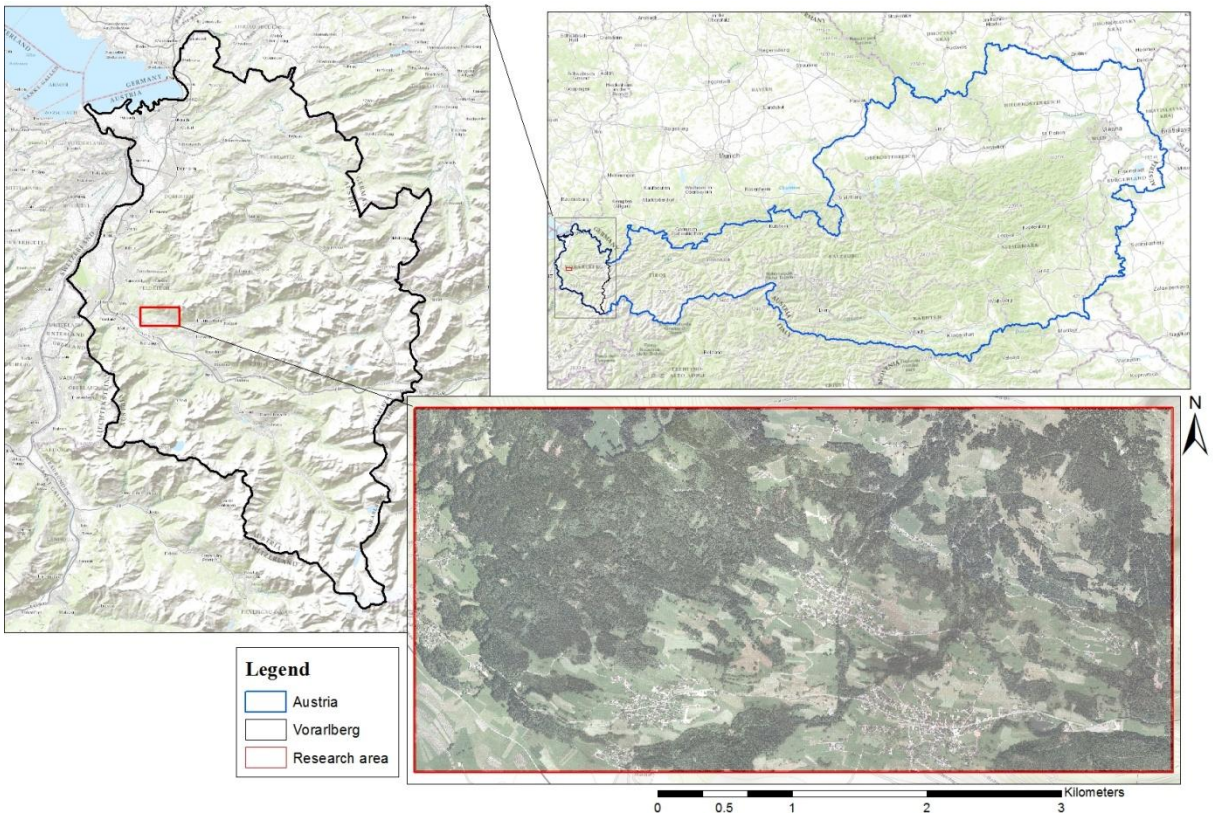

Figure 2.1 Overview of the research area in Vorarlberg, Austria. The right map shows an overview of Austria with the highlighted extent of the Federal State of Vorarlberg. The latter is enlarged on the left map. The extent of the study area is indicated with the red box.

2.1 Relief and climate

Figure 2.2 shows the relief of the research area by the 3D-representation of a digital elevation model (Land Vorarlberg, 2016). The largest part of the research area is situated at the border of the large valley between Feldkirch and Bludenz. However, in the northern, and especially the north-eastern, part of the area steep slopes account for a rapid rise of the surface elevation.

Figure 2.2. Relief of the research area, shown by a 3D-Digital Elevation Model (DEM), derived from Land Vorarlberg (2016).

The climate in Vorarlberg is characterized by high precipitation volumes and spatially heterogeneous amounts of rainfall due to the mountainous landscape (Markart *et al*., 2007; Lindenmaier *et al*., 2008). Generally, higher precipitation amounts are measured in the period between April and September, due to convective storm events enhanced by Lake Constance in the north-western part of Vorarlberg. During these periods, (thunder) storm events with 30-40 mm of precipitation within 12 hours are not uncommonly observed (Seijmonsbergen, 1992; Lindenmaier *et al*., 2008).

This study area is situated in the West-Vorarlberg region, which is characterized by a more temperate climate and lower amounts of precipitation compared to the north-eastern parts of Vorarlberg. Precipitation volumes are being measured at the weather station in Feldkirch, which is situated 439 metres above sea level and ~10 kilometres west of the study area, in which altitudes between 480 and 1800 metres can be measured. Figure 2.3 gives the monthly average precipitation - and temperature records from the Feldkirch weather station for the period 1961-1990.

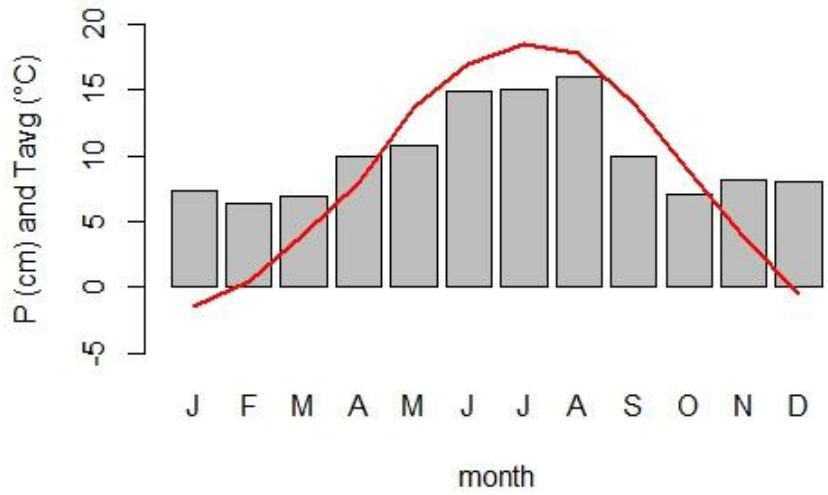

Figure 2.3. 30-year monthly average precipitation - and temperature records from Feldkirch Wetterstation for the period 1961-1990, derived from Markart *et al*., 2007. The bars show the monthly average cumulative precipitation volumes in centimetres, while the line shows the monthly average temperature in °C. The average annual volume of precipitation for this period is 1207 mm, while the average temperature in this period is 8.2°C.

This graph shows that the driest month, February, on average still has a precipitation amount of 64 mm. The wettest month, August, on average measures 160 mm of rain. The months January and December did have average temperatures below zero for this period.

The largest part of the study area is expected to have a similar annual precipitation pattern and total volume as presented in figure 2.3 (Seijmonsbergen, 1992). However, the total annual volumes of the northern- and especially the north-eastern mountain slopes are expected to be higher (1500-1700 mm), while the lowest south-western valley annually receives precipitation volumes between 1000 and 1250 mm (Seijmonsbergen, 1992).

The climatic snowline in the region around the study area is located at 2650 m (Seijmonsbergen, 1992). Since the highest part of the study area is located at 1800 m, it does not contain an area which is permanently covered with snow. Although there are no monthly snow records available for the study region, Seijmonsbergen (1992) stated that the average annual total snow depth in the valley between Feldkirch and Bludenz, to which a large part of the area belongs, is between 27 and 39 cm. This snow depth increases with altitude. For example, from snow records from Brand and Lünersee, which are located approximately 13 and 18 km south of the study region and have altitudes of 1037 and 1980 m respectively, average annual total snow depths of 79 and 287 cm are calculated (Seijmonsbergen, 1992).

2.2 Vegetation

Figure 2.4 shows the species map of Vorarlberg, cut out for this research area, of which the data can be downloaded on the GIS-information website of the Federal State of Vorarlberg (Land Vorarlberg, 2016). The data is based on field observations by students 'Biology' commissioned by the Department of Forestry of Land Vorarlberg (C. Hiebeler, personal communication, March 29, 2016) and comprehensive descriptions of each class are collected in Amann *et al*. (2014). Large polygons with different colours each represent a dominant species in that particular part of the forest.

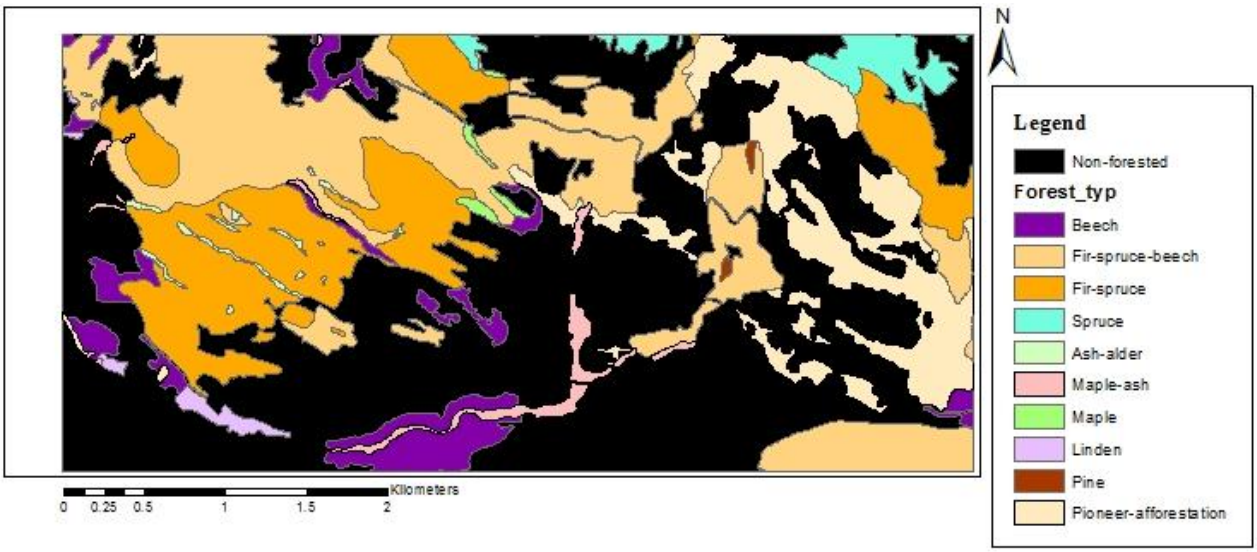

Figure 2.4. Species map of the study area, derived from Land Vorarlberg (2016) and Amann *et al*. (2014). The black areas represent non-forested areas, while each colour represents a certain classified forest type.

From this figure, it can be observed that the areas classified as 'fir-spruce-beech' and 'fir-spruce' cover the largest part of the forested area. These two classes together cover more than 5 km^2, which is

around one third of the entire study area (table 2.1). Adding the separately classified 'beech' and 'spruce' areas, these three species account for more than 6.1 km^2 of the total study area, which is more than 40% of the entire study area and more than three quarters of all the forested areas. Also the class 'pioneer-afforestation' covers a notable portion of the region (9.1%). This class consists of natural vegetation, which covers former abandoned meadows (~90%), and homogeneous afforested former meadows (~10%). The former natural vegetation is a mixed forest with amongst others birch, spruce, alder, hazel, larch, willow and beech. The homogeneous afforested areas consist mainly of spruce (Amann *et al*., 2014).

Table 2.1. The species classification of Amann *et al.* (2014) and Land Vorarlberg (2016) displayed by area in the study region.

Forest type	**Area (ha)**	**% of total**
Fir-spruce-beech forest	305.1	20.0
Fir-spruce forest	212.0	13.9
Pioneer-afforestation	138.9	9.1
Beech forest	67.2	4.4
Spruce forest	28.2	1.8
Maple-ash forest	20.9	1.4
Linden forest	8.1	0.5
Ash-alder forest	6.4	0.4
Maple forest	4.5	0.3
Pine forest	1.6	0.1
Total area	1526.5	100
Total forested area	792.7	51.9
Total non-forested area	733.8	48.1

3. Methodology

3.1 Rainfall interception model

In this study, the canopy interception was estimated using a theoretical interception model, which includes vegetation properties. This model is based on the assumption of an exponential relation to fill up the canopy storage with rainfall. The origin of this model was introduced by Horton (1919). He stated that interception loss was the sum of the water stored on the vegetation and the evaporation of the wetted plant surfaces during the storm (Merriam, 1960):

$$I = S + RE\Delta t \qquad \text{eq.1}$$

where I is the interception loss (mm) over the projected area of the canopy, S is the water stored on the plant surface at the end of the storm (mm) over the same projected area of the canopy, R is the ratio of evaporating surface to the ground projected area of the canopy, E is the rate of evaporation from the wetted vegetation surface (mm/hour) and Δt is the storm duration in hours. However, this equation does not describe the relation between the amount of rainfall (P) and the water stored on the plant surface (S). To describe this storage-precipitation relation, an exponential model was introduced by Linsley *et al*. (1949) and further developed by Merriam (1960):

$$I = S\left(1 - e^{-\frac{P}{S}}\right) + RE\Delta t \qquad \text{eq.2}$$

where P is the amount of rainfall in mm and the other parameters remain unaltered. Using this approach, the first term of the equation, the water storage on the plant surface, depends on the amount of rainfall (P) and can not be larger than S. Therefore, the term S should now be defined as the maximum storage of the plant surface or the storage capacity of a projected area of the canopy (mm). From now on, this term will be defined as S_{max}. Aston (1979) further modified the interception model, after the model was tested with laboratory experiments. In these experiments, high amounts of rainfall were simulated to water small trees and calculate the canopies' storage capacities. The measured interception was compared to the modelled interception using equation 2. Due to the high amounts of rainfall in a relatively short time period, the evaporation term in equation 2 was assumed to be negligible. The experiments showed that the storage on the plant surface was overestimated in almost all cases by the model. To obtain a reasonable fit, a factor k was added to equation 2. This factor has a value between 0 and 1 in order to reduce the calculated rain detention by the tree:

$$I = S_{max}\left(1 - e^{-\frac{kP}{S_{max}}}\right) + RE\Delta t \qquad \text{eq.3}$$

Aston (1979) stated that the factor k represents the proportion of rainfall that falls on the canopy. For very dense canopies, k approaches 1. Solving and applying k gave excellent agreement between the measured and calculated interception (Aston, 1979).

An explanation for such excellent agreement between the measurements and calculation of interception without the evaporation term is the use of high simulated rainfall intensities (22-52 and 72-98 mmh^{-1}), which are theoretically characterised by a relative unimportance of evapotranspiration (Aston, 1979). Aston (1979) stated that lower agreement would be expected when low rainfall intensities were used, because the plants would require larger times to reach canopy saturation and during this period, ambient air parcels would still be unsaturated which enables evaporation to occur. However, Lankreijer *et al*. (1999) stated that the evaporation rate during storms in general is very low. They claimed that the driving forces for evaporation during rainfall are limited because of the low level of available energy (due to cooling of the canopy) and the low level of vapour pressure deficit, especially during long showers.

The performance of equation 3 was tested in this study on plot-scale in the field, thereby especially focussing on species-specific vegetation properties. Because of the above mentioned theories of Aston (1979) and Lankreijer *et al*, (1999), the evaporation term in equation 3 was assumed to be negligible, thereby taking an uncertainty into account which especially applies for small rainfall events. S_{max} and k are properties of the vegetation structure, which can (in)directly be determined on plot-scale. The former parameter, S_{max}, depends on the leaf area and structure, which is in turn species-specific. Because the plot-scale leaf area index (LAI) could be estimated directly, a relation between the leaf area and S_{max} per species could be used to estimate S_{max} on plot-scale. Since these species-specific relations did not exist, these were first determined by fieldwork on branch-scale. The latter parameter, k, could, like the leaf area, be estimated directly from a plot, as canopy cover fraction. When these vegetation structure properties were determined for a certain plot, the canopy interception could be modelled for each precipitation volume. The modelled interception values were ultimately compared with field measurements of interception for the same plots. The details of this fieldwork methodology are described in the remaining part of this chapter.

An important objective of this study is to use this interception model, which includes the species-specific vegetation properties, to estimate the spatial variability of canopy interception on regional scale. De Jong & Jetten (2007) developed a method to quantitatively estimate canopy interception

from earth observation products, thereby using this exponential interception model and assuming a negligible influence of evaporation during the storm event. Because this model is now applied on a grid, instead of on a plot, an extra factor is added to the exponential model. The previous studies all calculated the interception over a projected area of the canopy. However, not each grid cell in a remote sensing image will be completely covered with canopy. The model would overestimate the interception for grid cells for which only a fraction is covered by canopy or do not contain any canopy at all. Therefore, a correction factor for the overall canopy cover fraction within a grid cell (C_p) is added to the exponential model:

$$I = C_p S_{max}(1 - e^{-k\frac{P}{S_{max}}}) \quad \text{eq.4}$$

De Jong & Jetten (2007) used the HyMap sensor for their study, which provides images with a spatial resolution of 5 by 5 m and contains information from 126 spectral bands. For remote sensing data with this resolution, calculating interception loss using equation 4 seems to be a very promising approach. The added C_p variable becomes especially important when the resolution is lower large grid cells contain more than one surface type.

However, in this study, very high resolution images (0.125m) are used, for which the details will be described in paragraph 3.3.1. Because we aimed to use species specific characteristics to calculate the canopy interception, a classification needs to be performed. Therefore, each grid cell was assigned to a certain class of land cover type. It should be noted that some grid cells which are not fully covered with canopy, are still classified as a certain tree species. On the other hand, it can occur that grid cells which do only contain a small fraction of canopy and a large fraction of bare soil, are classified as bare soil. Because only 'forested' grid cells are taken into account when calculating the interception, these small parts of vegetation canopies are lost in the model. However, the higher the resolution, the smaller the area size of this loss. Besides, a considerable portion of these lost pixels are returned into a 'forest species' class using the majority analysis approach, which will be described in the next paragraph.

Because of this species-specific approach, the C_p factor becomes only important in those grid cells which are classified as a certain forest type, but are not fully covered with canopy. However, using these high resolution images, the 'gaps' in the canopies can be determined directly much better compared to lower resolution images. This means that the overall fraction of vegetation cover within a grid cell can be determined directly, instead of first calculating the fraction of canopy cover within a grid cell (C_p) and subsequently correct for 'open areas' in the canopy (k). Therefore, the C_p-factor and k-factor are combined for this study into the factor c, which is defined as the overall vegetation cover fraction within a grid cell:

$$I = S_{max}(1 - e^{-c\frac{P}{S_{max}}}) \quad \text{eq.5}$$

The model which is used in this study to map the canopy interception is based on equation 5 and is built using the PCRaster 4.0.2 software (Karssenberg, 2014).

Since the precipitation volume of a storm event is assumed to be approximately constant in the entire study area, the largest variability in interception between the grid cells will occur due to variability in overall vegetation cover fraction within a grid cell (c) and variability in storage capacity of the canopy within a grid cell (S_{max}). The former parameter (c) is calculated in this study by combining information from the remote sensing imagery with the measurements of k on plot-scale in the field. Because the GPS-coordinates for each plot in the field were saved, the plot measurements of k were related to

remote sensing products for the same areas. This relation is used to calculate the overall vegetation cover fraction for each grid cell in the study area. The latter parameter (S_{max}) is dependent on the leaf area, as previously mentioned. Therefore, an estimation of LAI for each grid cell was made first, before the S_{max} could be estimated. This LAI estimation was based on a field-based relation between the canopy cover fraction and LAI. This relation is determined by plotting the estimated LAI's against the canopy cover fractions and fitting the Beer-Lambert equation through the points. The Beer-Lambert equation relates light transmittance under a canopy to the LAI by using a radiation extinction coefficient (Bolstad & Gower, 1990; Martens *et al*., 1993; Maass *et al*., 1995; Bréda, 2003). The equation has a logarithmic character and is assessed as a successful approach to determine LAI in many papers (e.g. Maass *et al*., 1995; Bolstad & Gower, 1990; Pierce & Running, 1988; Vose *et al*., 1995; Martens *et al*., 1993; Sampson & Smith, 1993; MacFarlane *et al*., 2007; Richardson *et al*., 2009). Using these species-specific relations between LAI and canopy cover fraction, the canopy cover fractions in the grid cells are converted to LAI values. Subsequently, these LAI values per grid cell are converted to S_{max} values, using the previously mentioned species-specific relations between S_{max} and leaf area on branch-scale. Finally, the S_{max}- and c-values for each grid cell are used to calculate the canopy interception, using equation 5 and a certain volume of rainfall. The used methodologies are described in detail in the remainder of this chapter.

3.2 Fieldwork

The fieldwork was performed during a three-week period in October 2015. Two fieldwork sites were selected. The first fieldwork site is situated in the forests between the villages of Düns and Dünserberg in the mid-eastern part of the entire research area. The second fieldwork site is situated in a small forest northeast of the village of Röns and southwest of the Düns (figure 3.1). The main reasons for the selection of these sites are the accessibility of the forests and the contacts with the local municipalities.

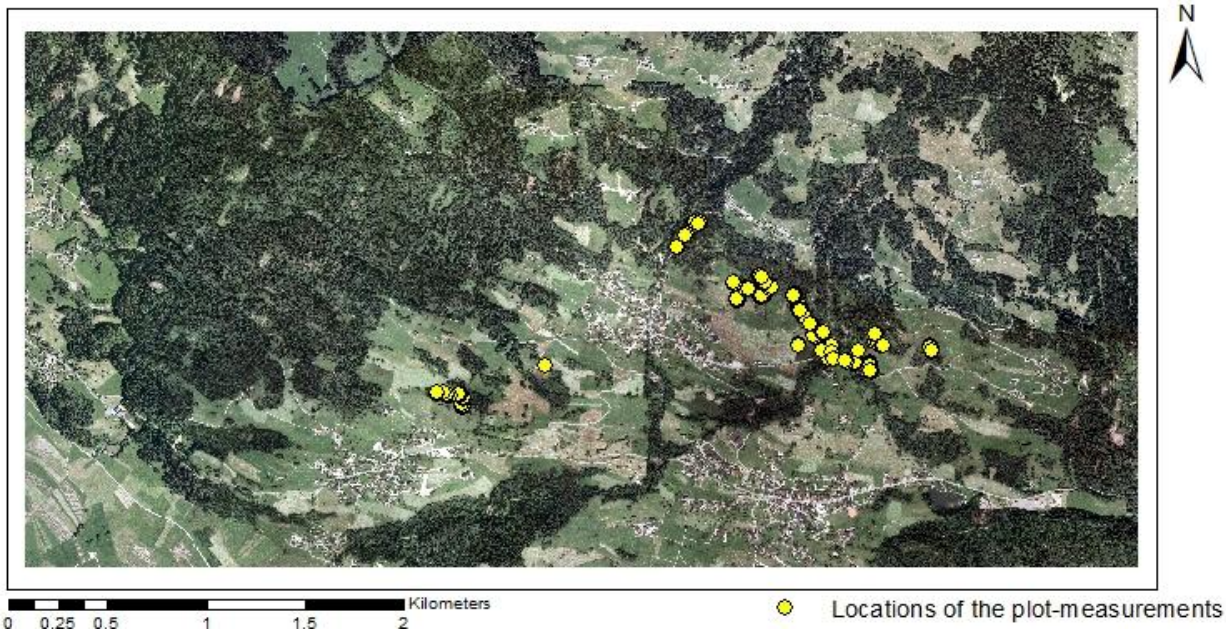

Figure 3.1. Fieldwork sites. The locations of the plot-measurements (5x5m) are highlighted with yellow dots. The first fieldwork site is located in the forests between Düns and Dünserberg (eastern site). The second fieldwork site is located between Röns and Düns (western site). The collection of branches for the storage capacity measurements was performed in the first fieldwork site.

3.2.1 Storage capacity - leaf area relations on branch-scale

The smallest-scale influence of vegetation on canopy interception is the influence of the leaf- and branch structure. The leaf- and branch structure strongly influences the degree to which water can be detained by the vegetation. Together with the amount of leaves and branches, which is defined as the leaf area, this structure determines the storage capacity (S_{max}) of the canopy. Because the leaf- and branch structure differs strongly between species and LAI has a strong spatial variability, S_{max} is expected to be far from constant in a natural mixed forest (Aston, 1979; Valente *et al*., 1997; Van Dijk & Bruynzeel, 2001; De Jong & Jetten, 2007). Since the interception does not exceed the storage capacity, the value of S_{max} is considered as the most important parameter in the exponential model (Aston, 1979). Therefore, a relation between the S_{max} and LAI was attempted to be found for each dominant species in the study area, using measurements on branch-scale in the field. The dominant species were selected only by field observation in the fieldwork area, because the existence of the species map from Land Vorarlberg (2016) was unknown for the author during the period of fieldwork.

From each of the five dominant species in the fieldwork area 30 branches from different sizes and with different leaf areas were cut. In order to calculate the leaf area per single branch, each branch was laid onto a large white sheet and photographed at least three times. It was attempted to keep the position of the camera vertically straight above the branch as much as possible. For the second and third photograph a tapeline was placed which stretched at least to the ends of the branch in the x- and y-directions respectively. Using the Adobe Photoshop CC 2015 software, the first photograph is cut in such a way that the ends of the branch touch the outlines of the cut image. Subsequently, the branch is made completely black, while the white sheet background is made completely white, using a colour range selection tool, see figure 3.2. Reading the fraction of black in the image and multiplying this with the actual dimensions of the image in reality, which were read from photograph 2 and 3, the total leaf area was calculated. It was attempted to select branches which do contain the least overlapping leaves, so that the real leaf area could be estimated. However, the larger the branch, the more difficult this approach is and the less accurate the leaf area determination will be.

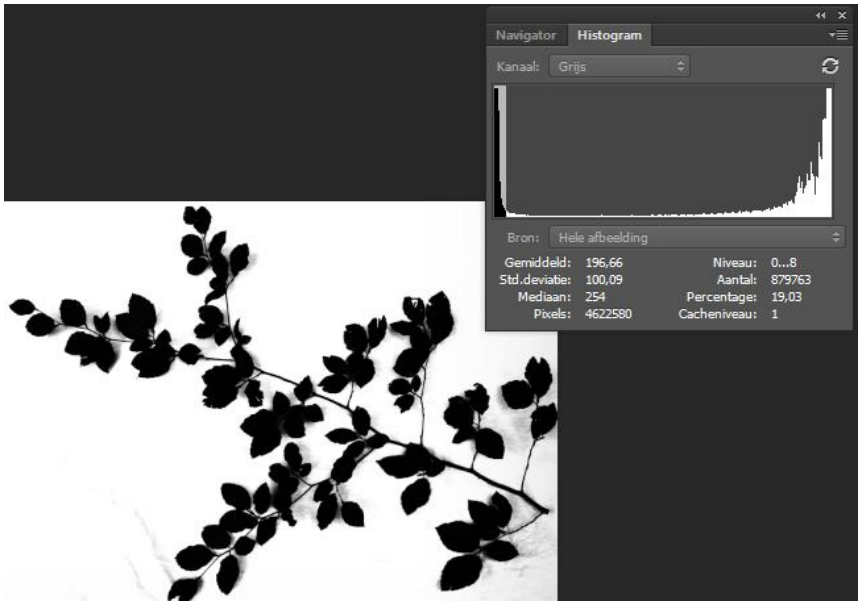

Figure 3.2. Screenshot of the colour range selection tool in the Adobe Photoshop CC 2015 software during the branch analysis. The histogram in the top-right part of the figure shows that the software can make a clear distinction between the branch (black) and the background (white).

To determine S_{max}, each branch was weighted individually with a KERN HDB 10K10 digital hanging steelyard balance with an accuracy of 10 g. The branches were horizontally placed into a net, mimicking the natural position of a branch as good as possible. Each branch was weighted again in a completely wet situation after watering the branch with a watering can. From Aston (1979) it follows that the time that the storage capacity reaches a maximum is shorter when watering intensity is higher. Therefore, the branches were being watered with a very high watering intensity of about 5 litres in 30 seconds. The wet weight of the branch and the net together was read at the moment the branch and the net just stopped dripping to minimize the influence of evaporation after the 'event'. The wet weight of the branch was subsequently determined by subtracting the weight of the wetted net from the total weight. Subtracting the dry weight from the wet weight gives the S_{max} in grams, which is converted to cm^3 and eventually to mm.

The S_{max} values were plotted against their corresponding leaf areas. Species-specific relations between S_{max} and leaf area were determined using a simple linear regression approach.

3.2.2 Canopy cover fraction and LAI

Because it was aimed to test the interception model with measurements on plot-scale, rather than only on branch-scale, both the storage capacity as the canopy cove fraction were determined on plot-scale. Moreover, it was required to link plot-scale canopy cover fractions and LAI's to remote sensing products as will be described in the remainder of this chapter. Therefore, 50 square plots of 5 by 5 m selected in the fieldwork area, each solely covered by one of the five dominant species. Because of the dominance of just a few tree species, together with a limited period of fieldwork, only plots which are covered with one of the five most dominant species in this fieldwork area were measured during the fieldwork campaign. It is the author's estimation that these five species cover at least 80% of the fieldwork area. The particular species of each plot was noted and the coordinates were saved with a Garmin GPS 72H GPS device. The saved waypoints had an accuracy of 3-9 m.

A considerable part of the measurements on plot-scale, was the hemispherical photography. The canopies above the 5 by 5m plots were photographed using a Canon EOS 350D Digital camera with a fish-eye lens, for the purpose of calculating the canopy cover fraction and the leaf area index. Several studies, including Chen *et al*., 1997; Van Gardingen *et al*., 1999; Jockheere *et al*., 2004; Zhang *et al*., 2005; Morsdorf *et al*., 2006 and Zhou *et al*., 2010 claim that this hemispherical photography analysis is a well suited method to calculate LAI and canopy cover fraction.

The camera was horizontally levelled on the forest floor using a hard cover notebook and a spirit level, with its lens towards the sky. Pictures have been made on five places in each plot: in the centre of the plot and on the lines between the centre and each corner, 20-30 cm from the corner. For each plot, the canopy cover fraction was calculated using the Can-EYE v6.314 imaging software. This Can-EYE software is designed to process multiple pictures at once and to derive information from those pictures such as the LAI and the canopy cover fraction (Weiss & Baret, 2010). Instead of using the entire 180° angle of view for the images analyses, the circle of interest is set to 60° by default, because of larger occurrence of mixed pixels in the image regions with zenith angles > 60° (Weiss & Baret, 2010). Can-EYE uses a classification tool for the calculation of canopy characteristics based on colours in the image. For this study, a 2-classes classification is performed. The pixels which belong to the 'sky' are recognized by the program and further corrected manually. The remaining pixels are assigned to the 'vegetation' class. An example of the image classification process by Can-EYE is given in figure 3.3. The figure shows on the left side the ten hemispherical photos in the plot (two pictures per location) and on the right side the classification by Can-EYE. The green areas are the vegetated areas and the blue areas is the sky.

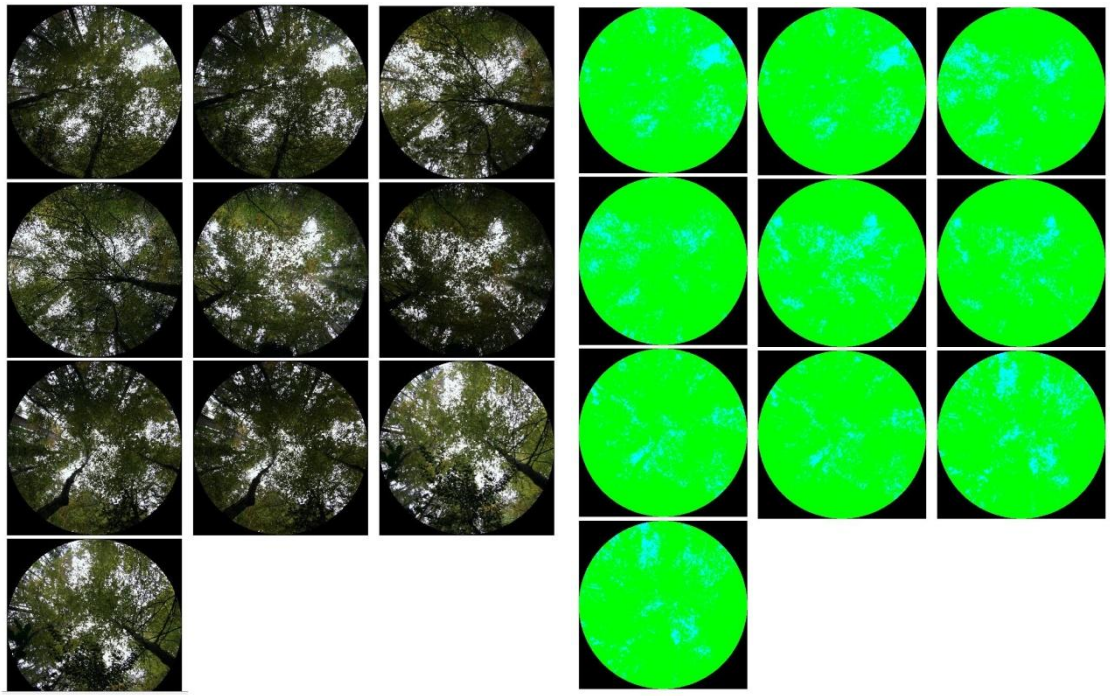

Figure 3.3. An example of the image classification process of a *Fagus sylvatica* (beech) plot by Can-EYE. The left part of the figure shows the original hemispherical photographs for a 60° circle of interest, while the right part of the figure shows the classification of sky (light blue) and vegetated areas (green) by Can-EYE.

Subsequently, Can-EYE calculates the canopy cover fraction using the following equation:

$$fCover = 1 - P_o(0) \qquad \text{eq.6}$$

where fCover is the canopy cover fraction and $P_o(0)$ is the 'gap fraction' in the zenith direction. The gap fraction is generally defined as the fraction of view that is unobstructed by canopy in any particular direction (Welles & Cohen, 1996), which is equal to the sky when the observer looks upward from under the canopy. However, because hemispherical images are used for the calculation of the canopy cover fraction, it is not possible to get a value in the exact zenith direction. Therefore, CAN-EYE integrates the canopy cover fraction over a range of nadir angles, which is set to 0-10° (Weiss & Baret, 2010).

The same hemispherical photographs were used to assess the LAI per plot. Can-EYE estimates the LAI using the gap fractions in the hemispherical photograph series. A database of gap fractions is built for a large range of random combinations of LAI with values between 0 and 10 (steps of 0.01), using a Poisson model. The Poisson model is an exponential relation between the gap fraction and LAI, thereby using a clumping parameter and a projection function and correcting for the angle with respect to zenith. The LAI for the series of images from one plot is directly read from the database for the gap fractions calculated from the plot images. The LAI which is calculated using this equation is the effective LAI, which assumes no foliage clumping. However, for a heterogeneous and clumped canopy, the effective LAI needs to be converted into the true LAI (Ryu *et al*., 2010). Can-EYE uses a clumping parameter for each zenithal ring for this conversion, which is based on the assumption that vegetation elements are locally randomly distributed and is derived from the images itself (Weiss & Baret, 2010).

The method of processing hemispherical images which is performed by Can-EYE actually estimates the plant area index (PAI), instead of the LAI. Since some parts of the image are covered with stems

and trunks instead of leaves, it is not possible to find out whether there are leaves present behind the stems and trunks. Masking out these stems and trunks could give a large underestimation of the actual LAI (Weiss & Baret, 2010). This should be taken into account when interpreting the results.

3.2.3 Interception measurements

After the species-specific leaf- and canopy structures, represented by S_{max} and k, were determined for fifty plots, the canopy interception could be estimated for these plots using equation 3 and a certain input volume of precipitation. To test the performance of the interception model, the interception was indirectly measured in a couple of plots.

Because the mass balance of interception is generally expressed as in equation 7 (Crockford & Richardson, 2000), and interception cannot be measured directly on plot-scale, both the gross precipitation and throughfall are measured to determine interception.

$$I = P - T - S \qquad \text{eq. 7}$$

where I is interception, P is gross precipitation, T is throughfall and S is stemflow.

The contribution of stemflow to this mass balance is assumed to be negligible in this study for the following reasons. First of all, the fraction of gross precipitation which ends as stemflow is generally estimated to be quite low. Most studies measured stemflow as being lower than 2% of the gross precipitation (e.g. Asdak *et al*., 1988; Lloyd *et al*., 1988; Hutjes *et al*., 1990; Veneklaas & Van Ek, 1990; ; Sinun *et al*., 1992; Lorens *et al*., 1997). However, other studies estimate the amount of stemflow to be 6-9% of the gross precipitation (Kelliher *et al*., 1992; Crockford & Richardson, 2000) or even 13.1% of precipitation events larger than 25 mm (Crockford & Richardson, 2000). Certainly, the magnitude of the fraction of gross precipitation which becomes stemflow depends strongly on species because of the branch pattern and is lower for higher rainfall intensities and larger LAI's (Crockford & Richardson, 2000). Secondly, the accuracy of the throughfall measurements is not high enough for stemflow to be a significant contributor to the mass balance. Besides, the measurement of stemflow is relatively difficult and time-consuming. The assumption of a negligible stemflow should be taken into account when interpreting the results.

The throughfall is measured in three plots: one *Fagus sylvatica* plot and two *Picea abies* plots. These plots were selected because of their accessibility and perfect species homogeneity. Unfortunately, there was some delay of the delivering of the more sophisticated rain gauges. Therefore simple rain gauges were constructed using soda bottles from the same brand. The upper parts of the bottles were cut off at the same levels and replaced upside down onto the lower part of the bottles after these were made heavier with pebbles, to minimize to influence of evaporation.

Twelve rain gauges were made using this method from which eleven were placed under the canopy to measure throughfall and one was placed in an open field nearby to measure the gross precipitation. The rain gauges under the canopy were randomly placed within the borders of the plots and horizontally levelled using a spirit level. After each storm event, the volumes of rainwater within the rain gauges were measured and the gauges were emptied. Because the areas of the rain gauges were calculated, the amount of measured rain could be converted from litres to millimetres.

Eventually, the interception values for the three plots could be compared to the interception calculations using equation 3 and the vegetation characteristics of the same plots described in the previous paragraphs.

3.3 Remote sensing

In this study, high-resolution remote sensing imagery was used for the quantitative estimations of the spatial variability of canopy interception on regional scale. The previously mentioned species-specific leaf- and branch structures were upscaled to a regional scale using products from this imagery.

3.3.1 Airborne imagery

The most recent aerial photographs for this area, orthophotos from 2012, were used for this study. These images contain information derived from the RGB-part of the electromagnetic spectrum with a resolution of 12.5 cm. A mosaic of aerial photos from different flights covers the whole federal state of Vorarlberg. Photos from different flight moments are projected within the extent of this study region and the different timing has an effect on the image analysis. Figure 3.4 shows the parts of the study area which have different flying moments. The flight moment of the green part of the study area was around 9 am on June 16, 2012. The purple parts were photographed around 10 and 11 am on June 28, 2012 and the flight moment of the areas displayed in red was around 11 am on August 19, 2012 (S. Martin, personal communication, February 5, 2016).

Together with the images from 2012, orthophotos from 2001, which contain information from a spectral band in the NIR region, were used for species classification. These images have a resolution of 25 cm and parts of the study area with different flying moments are shown in figure 3.5. The green areas represent the data from the first flight moment, which was on July 22, 2001 (unknown time) and the second flight date represented by the red colour was August 14, 2001 (unknown time).

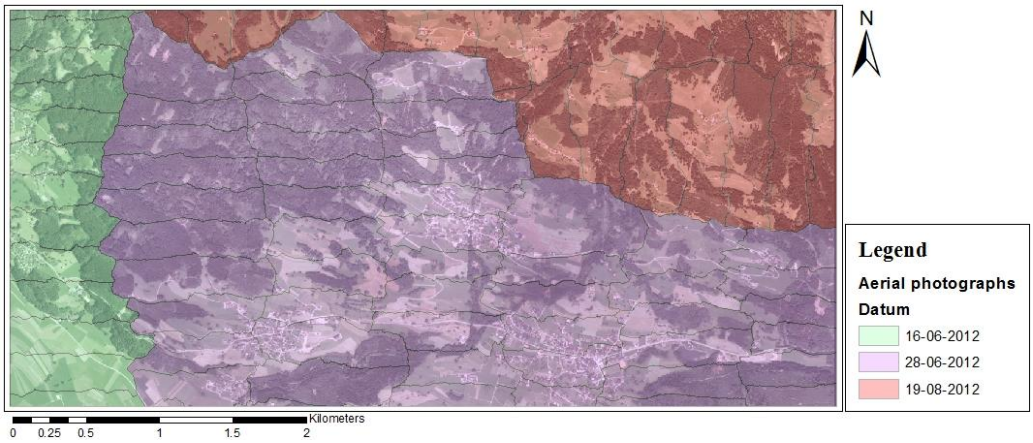

Figure 3.4. Fractions of the 2012-image separated by flight dates.

Figure 3.5 Fractions of the 2001-image separated by flight dates.

The spectral sensitivities of both the cameras which are used in 2001 and in 2012 are given in table 3.1. The three spectral bands of the 2012-image have spectral sensitivities which lie in the blue, green and red part of the electromagnetic spectrum. On the other hand, the spectral bands of the 2001-image are sensitive in the green, red and near-infrared part of the electromagnetic spectrum.

Table 3.1. Spectral sensitivity per camera (Source: Álvarez *et al.*, 2010; USGS, 2010).

Band no.	**2012 (Vexcel Ultracam Xp -RGBI)**	**2001 (Zeiss RMK TOP 30/23 camera with a KODAK AEROCHROME III Infrared Film 1443 strip)**
1	B (400-600 nm) -centred on 470 nm-	G (400-600 nm) -centred on 550 nm-
2	G (480-660 nm) -centred on 550 nm-	R - (560-680 nm) -centred on 650 nm-
3	R (580-720 nm) -centred on 640 nm-	NIR - (600-850 nm) -centred on 850 nm-

3.3.2 Vegetation species map

In chapter 2, a vegetation species map was shown which was derived from GIS-data from Land Vorarlberg (2016) and information from Amann *et al.*, (2014). Using a species map is essential for this study, since all the leaf- and canopy structures are species-dependent. However, the existing map from Land Vorarlberg (2016) uses classes with combined species, for example the 'fir-spruce-beech' class. Since especially beech leaves have a completely different structure than the coniferous needles, this classification is too coarse for the purpose of this study. Therefore, a new high-resolution species classification map was created using both remote sensing imagery and field observations.

The different surface types in the study area were distinguished by means of a supervised classification. This supervised classification is based on the spectral differences between each species. Since the difference in reflectance between species (especially between coniferous and deciduous trees) is the largest in the near-infrared (NIR) part of the electromagnetic spectrum (Williams, 1991; Van der Meer & De Jong, 2011), both the information from the ortho photos from 2001, which contain a NIR band, and from the ortho photos from 2012, which show the most recent land cover, are included in the classification process.

The image processing is performed using the ENVI 5.2 software. First, the three layers (each representing one spectral band) of the 2001 image and those of the 2012 images were stacked, so that the reflectance spectra of the land cover types can be distinguished using six spectral bands. Next, both images were resized to a 1 meter resolution, mainly because of the highly detailed shadows, which complicate the classification. Besides, one of the purposes of this study is to make a model which can be implemented in the stability model of the BioSLIDE project, which runs on a lower resolution.

The next step was to create training areas for each species and for all other dominant land cover types, which serve as end-members for the classification process. These end-members were partly constructed using ground-truth data. The GPS waypoints were plotted in the image and polygons were drawn at the positions of the waypoints which represent the field plots. Each polygon was allocated to a previously indicated class, the end-members. Besides the five tree species, end-members were made for meadows, water, bare soil, roads, buildings, agricultural crops, two types of shaded areas and cleared forest. The shadows that the images contain show for a considerable proportion the shadow over 'open land'. This means the shadow of trees or buildings over grassland or open areas in the forest. A small part of the shadows were shadows within the forest, for example trees overshadowing understory vegetation or smaller trees. The latter shadows were partly removed by the Majority Analysis, which will be described below. Partly these shadows on understory vegetation or smaller trees remain in the image, and therefore are misclassified. The first class of shadows can be observed

as shadows in both images. The second shadow class are shaded areas in the 2001 image, but non-shaded areas in the 2012 image. Finally, the 'cleared forest' class is characterized by areas that were forested in 2001, but which are open areas due to forest clearing in 2012.

Subsequently, the actual classification was performed using the maximum likelihood classifier method, which is proven to be a successful method for tree species classification (Martin *et al*., 1998; Yu *et al*., 2006). Using this maximum likelihood classifier method, each pixel is allocated into one of the defined classes based on spectral similarity.

After the classification, a majority analysis was performed. This analysis changes spurious pixels within a large single class into that class, under the assumption that the pixels are incorrectly categorized. Misclassified pixels and shaded parts within a single tree were filtered out, using this tool. Also, a portion of the partly vegetated pixels which are classified as bare soil or shadow are reclassified as being part of a particular species.

Finally, the non-forest classes were combined into one single class, 'non-forested area', since the only focus of the model will be on forested areas.

3.3.3 Overall vegetation cover fraction map

As explained in paragraph 3.1, the factor c in the model is defined as the overall vegetation cover fraction within a grid cell. In a grid cell which is fully covered by trees, this equals the canopy cover fraction, which is measured in the field for each plot. Hence, if the field measurements of October 2015 could be related to a product of the 2012 RGB-images which approaches a description of vegetation cover, a c-map could be created. The method which was used to determine such a description of vegetation cover is the spectral mixture analysis approach. This approach, previously used by e.g. De Jong & Jetten (2007) is a method to receive the 'real' information from mixed grid cells. When a grid cell is composed by more than one surface type, unmixing of such a grid cell gives the 'real' fractions of each surface type within that grid cell. The pure reflectance values of the possible surface types need to be selected as end-members for the unmixing process. Considering a summer forest grid cell, three possible land use types could be found: green vegetation, forest floor and (heavily) shaded forest floor. Therefore, these three land use types were selected as end-members for this study. The 'lost' information due to the lowering of the resolution to 1m can therefore be restored. The type of unmixing which is used for this study is linear spectral unmixing.

The end-members were created by selecting the purest possible training areas of green vegetation, not-shaded -and shaded forest floor from the image itself. After the unmixing, each grid cell contained information about the fractions of the three end-members within that grid cell. The fraction of green vegetation in each grid cell is used for the canopy cover analysis. The training areas for all projected plots, which are described in paragraph 3.3.2, were 'recalled' and for each plot, the average fraction of green vegetation was calculated. Because most forested grid cells are made up of the selected end-members, most of the fraction values for green vegetation, forest floor and shaded forest floor are between 0 and 1. However, some of the unmixing results still are below 0 or above 1.

Finally, the average fractions of green vegetation derived from linear spectral unmixing were related to the canopy cover fractions of the corresponding plots, calculated from hemispherical photographs in the field. The species specific relations were used to convert the results of unmixing into a c-map. Those values of c which exceed the below 0 - or above 1 thresholds are manually cut to 0 and 1.

3.3.4 Leaf Area Index - and Storage Capacity maps

The c-map which is described in the previous paragraph is converted into a LAI map using the Beer-Lambert equation, which is fitted with the fieldwork results. This Beer-Lambert equation is based on the relationship between leaf area and light transmittance and is given below:

$$\frac{Q_i}{Q_o} = e^{-k*LAI} \quad \text{eq.8}$$

where Q_i represents the sub-canopy diffuse and direct radiation, Q_o is the above-canopy radiation and k is the radiation extinction coefficient (Bolstad & Gower, 1990; Maass *et al*., 1995). The Q_i/Q_o term can also be defined as the fractional light transmittance of the canopy, which is inversely related to the fractional light absorbance by the canopy or the fractional vegetation cover. Therefore equation 8 can also be written as

$$1 - fCover = e^{-k*LAI} \quad \text{eq.9}$$

and rewritten as

$$LAI = \frac{-\ln(1-fCover)}{k}. \quad \text{eq.10}$$

Although the Beer-Lambert equation is a simple model which assumes a homogeneous canopy and requires an estimation of k, accurate measurements of LAI have been obtained using this equation (Bolstad & Gower, 1990).

The field measurements of LAI were plotted against the corresponding field measurements of canopy cover fraction for each species. Subsequently, the LAI was calculated for the measurements of the canopy cover fraction using the Beer-Lambert equation, thereby using a random value of the extinction coefficient k. The latter was solved for each species to get the best fit, using the least-squares method. The resulting equations were used to convert the c-map into a LAI map.

Finally, this LAI map was converted to a S_{max} map using the relations between S_{max} and leaf area, assuming that the relations on branch-scale also exist on grid cell-scale.

4. Results

The objectives of this study are twofold. First, it was attempted to find out the influence of species-specific differences of leaf-and canopy structures on the interception process. This objective was attempted to be achieved by the analysis of fieldwork results. These results are presented in paragraph 4.1, which starts on branch-scale and ends on plot-scale. Second, it was studied whether these differences could be implemented into a high-resolution remote sensing imagery based model and what their influences were on the spatial variability of canopy interception on regional scale. The results of the latter objective are partly presented in paragraph 4.2. This paragraph is subdivided by components of the interception model. The last paragraph presents the results of the final high-resolution interception model.

4.1 Fieldwork results

4.1.1 Storage capacity - leaf area relations on branch-scale

The results from the field measurements on branch-scale are presented in figure 4.1. The dominant species in the fieldwork area for which these measurements are performed are *Picea abies* (Norway spruce), *Abies alba* (European silver fir), *Fagus sylvatica* (beech), *Quercus robur* (English oak) and

Pinus sylvestris (Scots pine). Following table 2.1, these species cover at least 77.5% of the total forested research area.

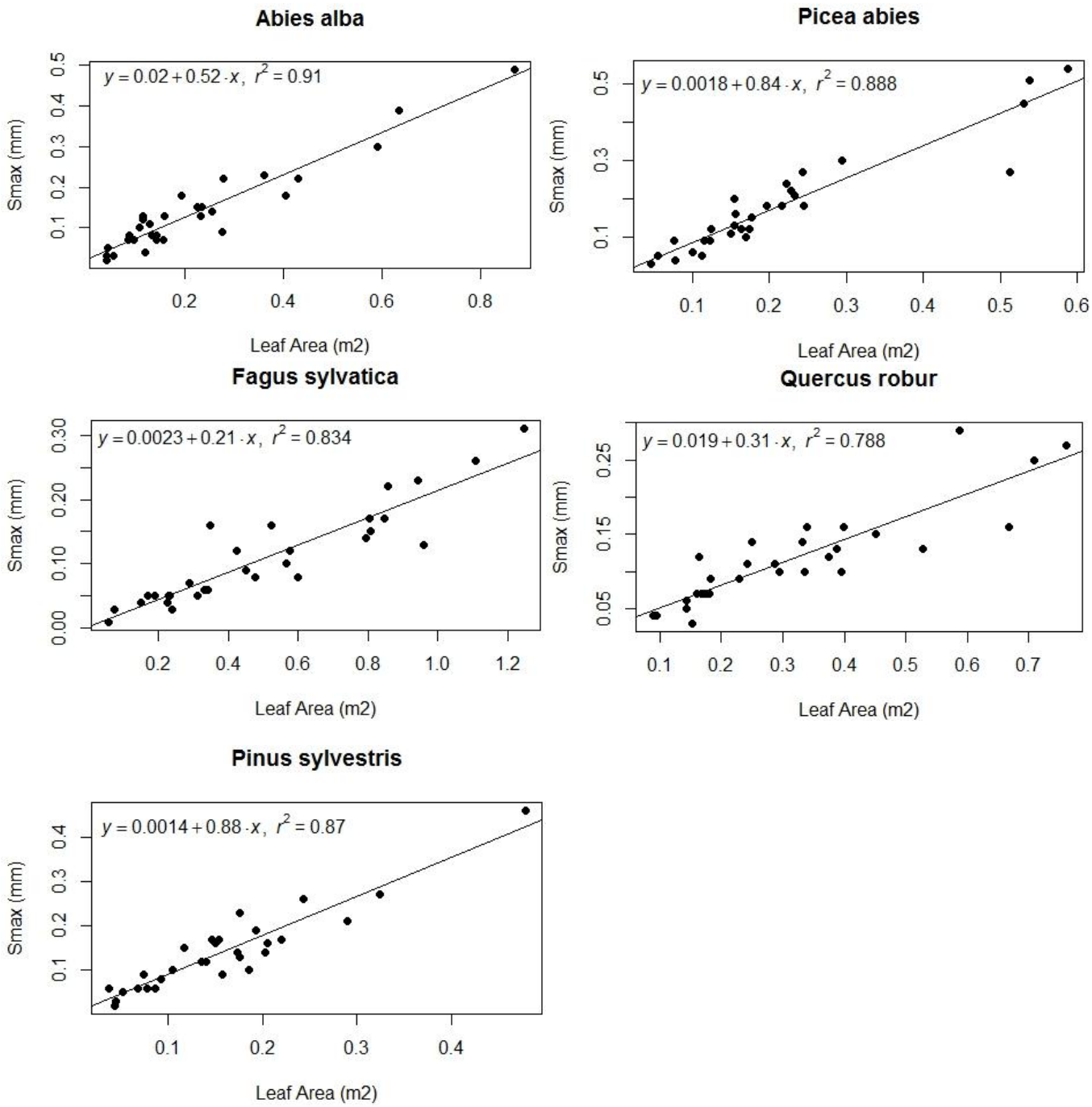

Figure 4.1. The species-specific relations between S_{max} (mm) and leaf area (m^2). The relations are based on field measurements on branch-scale. The dots represent the field measurements of S_{max} and leaf area, while the line shows the linear regression for these measurements. Both the regression equations and the r^2-values are presented in the plots.

Relatively high correlations can be found between S_{max} and leaf area for all five species. Considering the slope of the regression line equations, it appears that much more water can be detained by the coniferous species (*Picea abies*, *Pinus sylvestris* and *Abies alba*) for the same increase in leaf area than by the deciduous species (*Fagus sylvatica* and *Quercus robur*), especially for larger leaf areas.

Pinus sylvestris and *Picea abies* detain the water droplets more efficient when it comes to leaf area, detaining maximum amounts of 0.88 and 0.84 mm respectively for each square metre increase of leaf/needle area. The two coniferous species are followed by the *Abies alba*, which maximum water storage capacity is 0.52 mm per square metre increase of leaf/needle area. The slopes of the deciduous species *Quercus robur* and *Fagus sylvatica* are much smaller: for each squared metre increase of leaf area, an extra maximum amount of respectively 0.31 and 0.21 mm of water can be detained.

4.1.2 Canopy cover fraction and LAI (Beer-Lambert)

The imaging software Can-EYE v6.314 estimated the canopy cover fractions and the LAI using the hemispherical photographs from the field. These estimations were used to assess a logarithmic relation, based on the Beer-Lambert law. The results are presented in figure 4.2.

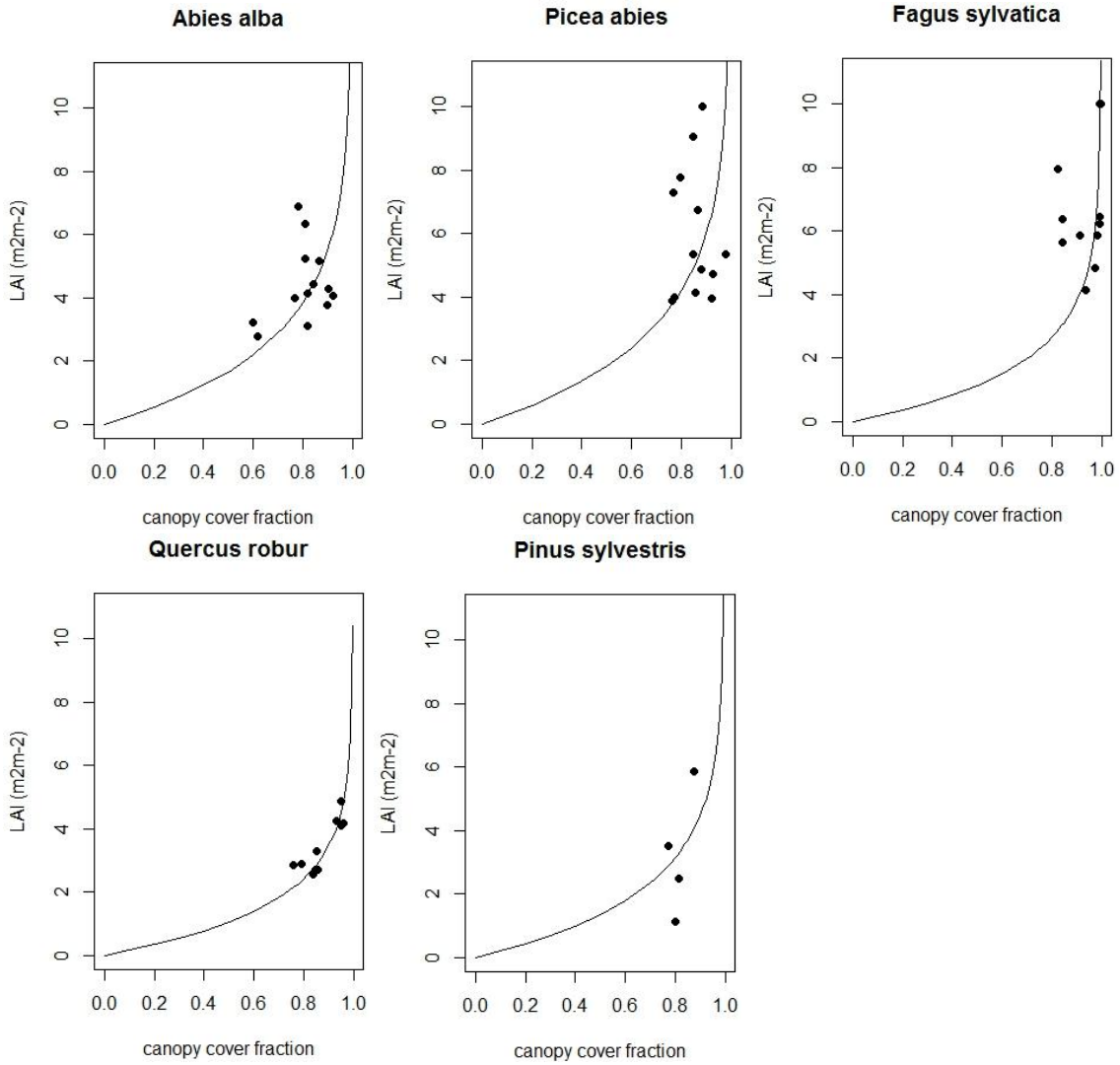

Figure 4.2. LAI-canopy cover fraction relations per species. The dots represent the field calculations of LAI and canopy cover fraction by Can-EYE, while the line represents the least-squares fitted Beer-Lambert relation.

The dots in the graphs above represent the field measurements, while the lines show the plotted Beer-Lambert equations, for which the extinction coefficients were solved for each species. The solved species specific Beer-Lambert extinction coefficients are presented in table 4.1.

Table 4.1. Extinction coefficients per species

Species	Extinction coefficients
Abies alba	0.418
Quercus robur	0.664
Fagus sylvatica	0.607
Picea abies	0.384
Pinus sylvestris	0.513

From the above can be observed that the deciduous species do have a clear higher extinction coefficient than the coniferous species. Especially the field observations of the *Quercus robur* fit well with the least squares fit of the Beer-Lambert equation.

4.1.3 Interception measurements

The canopy interception was estimated on plot-scale for three plots, using the relations between leaf area and S_{max} presented in figure 4.1, together with the results from the hemispherical photograph analyses. For the three same plots the actual canopy interception was measured. The characteristics of the three plots which were used for this analysis are presented in table 4.2. The canopy cover fractions and LAI-values were determined the processing of hemispherical photographs by Can-EYE. The S_{max} values were calculated with the S_{max}- leaf area relations given in figure 4.1, thereby using the LAI from the image processing.

Table 4.2. Characteristics of the interception measurement plots. The LAI- and c- values are determined by hemispherical image analysis and the S_{max}-values are subsequently calculated using the S_{max}-LAI relation determined from field measurements on branch-scale.

	Plot 1	Plot 2	Plot 3
species	Fagus sylvatica	Picea abies	Picea abies
canopy cover fraction	0.935	0.928	0.772
LAI (m^2m^{-2})	4.12	4.72	3.98
S_{max} (mm)	0.87	3.97	3.35

During the 3-week period of fieldwork in October 2015, there were only three storm events with measurable rainfall. The open field rain gauge measured cumulative amounts of rainfall of 20.2, 6.7 and 13.5 mm for these three storm events. The canopy interception values in the plots for each storm event, calculated by subtracting the measured throughfall from the measured open field rainfall, are given in table 4.3. The canopy interception values which are calculated with the exponential model (equation 5), thereby using the plot characteristics from table 4.2, are also presented in table 4.3.

Table 4.3. An overview of both the measured - and modelled interception values for the given storm events.

	Event 1 (P=20.2 mm)			Event 2 (P=6.7 mm)			Event 3 (P=13.5 mm)		
	plot 1	**plot 2**	**plot 3**	**plot 1**	**plot 2**	**plot 3**	**plot 1**	**plot 2**	**plot 3**
$I_{measured}$ (mm)	5.0	6.7	3.4	3.4	5.7	2.8	2.5	8.0	5.0
$I_{modelled}$ (mm)	0.87	3.93	3.31	0.87	3.14	2.64	0.87	3.8	3.2

As becomes clear from table 4.3, there are quite some differences between the measured - and modelled interception. The model did only perform well for events 1 and 2 in plot 3. In all cases the interception was underestimated by the exponential model. Strikingly, the measured interception values from plot 2 and 3 for event 3 are higher than those from event 1, while the open field rainfall

was clearly lower. Finally, in all cases the *Fagus sylvatica* modelled interception values were equal to the S_{max} value.

To check whether these model results could be improved, the three main uncertainties are summarized below.

1. It might be the case that the relations between S_{max} and leaf area on branch-scale can not be upscaled to a larger plot-scale

2. The Can-EYE estimations of LAI and canopy cover fraction might be too far from the actual values

3. The exponential interception model might be unsuitable for estimating canopy interception

Since the first and third uncertainties cannot be adjusted in case of incorrectness within the scope of this study, only the second uncertainty is analysed.

Assuming that the calculation of the canopy cover fraction by Can-EYE approaches reality (because the classification results were good and the method is straightforward), it was tested whether the estimated LAI-values could be the cause of the mismatch of the model with reality. The largest storm event, event 1, with a gross precipitation of 20.2 mm had the highest precipitation intensity and therefore is expected to give the best match with the conditions for the exponential model. Therefore this event was used to validate the model. New LAI-values were calculated for each plot, using equation 10 and solving the extinction coefficient k for a least-squares model fit to the interception measurement results. The resulting solved extinction coefficients and corresponding LAI values for this analysis are presented in table 4.4.

Table 4.4. The solved extinction coefficients and corresponding LAI-values for the exponential model fit to the interception measurement results for storm event 1 (P=20.2 mm)

	plot 1	**plot 2**	**plot 3**
Extinction coefficient (k)	0.111	0.303	0.366
LAI	24.7	8.7	4.0

Comparing the extinction coefficients from this table with those used in table 4.1 (0.607 for *Fagus sylvatica* and 0.384 for *Picea abies*), one can observe that especially the *Fagus sylvatica* extinction coefficients do not match. Using an extinction coefficient which is as low as this one gives extremely high LAI values. Considering the *Picea abies*, it holds that a small modification of the extinction coefficient in the model leads to changes in LAI for which the model does fit well with the field experiments.

However, since canopy interception measurements are complex, using these low number of field experiments of canopy interception for the modification of the k-values would be unreliable. Therefore, these results will not be implemented in the model results in the next paragraph.

4.2 Remote sensing results

4.2.1 Vegetation species map

The result of the species classification process using remote sensing imagery is given in figure 4.3. The black areas represent the non-forested areas, which is a combined class of all non-forest land cover types. The five different colours represent the five dominant species which were measured in the field. A magnification of this species map is given in Appendix A.

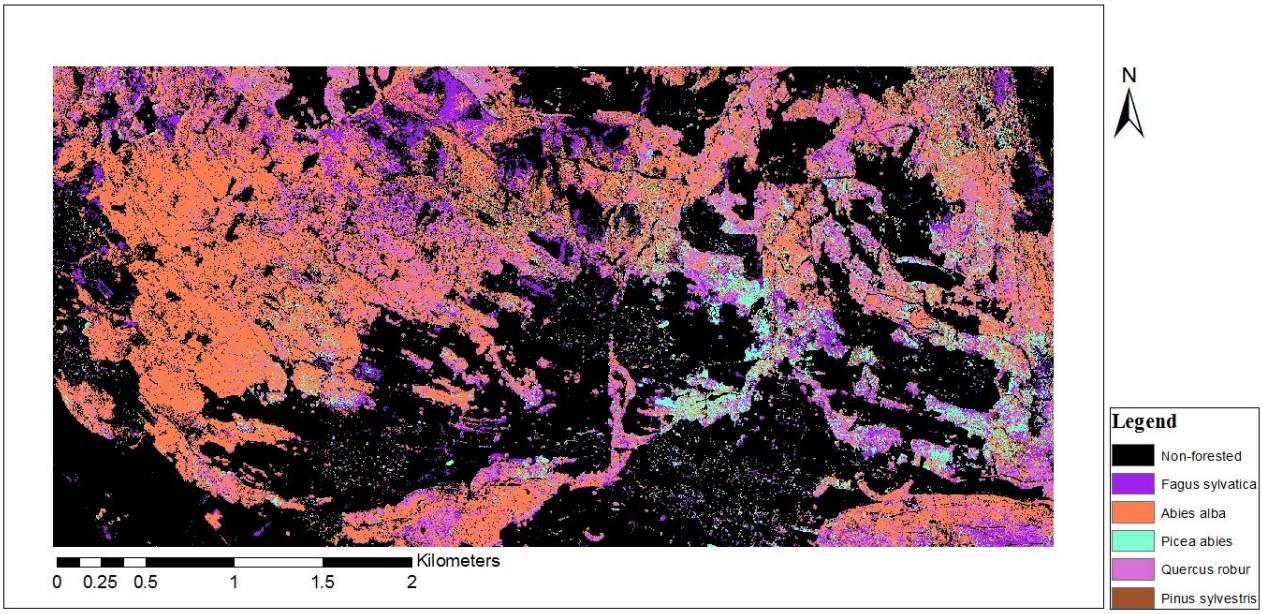

Figure 4.3 Species classification map, based on field observation and remote sensing imagery. The black parts of the image show the non-forested areas and each colour represents a different classified tree species.

Table 4.5 gives the corresponding absolute and relative areas covered per species, calculated by ENVI 5.2.

Table 4.5. Area covered per tree species, derived from the species map.

Forest type	**Area (ha)**	**% of total**
Abies alba	382.9	25.1
Quercus robur	141.5	9.3
Fagus sylvatica	115.8	7.6
Picea abies	88.3	5.8
Pinus sylvestris	38.9	2.5
Total area	1526.2	100
Total forested area	767.4	50.3
Total non-forested area	758.7	49.7

As can be observed from both figure 4.3 as table 4.5, the *Abies alba* is the most dominant species in this study area, with a coverage of more than 25% of the total study region. Especially in the western part of the study area, this dominance is clearly visible. The eastern part of the study area contains more diversity, without the dominance of one particular species. The fieldwork area is, as expected, characterized by a dominance of the *Picea abies* species. The least common species turns out to be the *Pinus sylvestris*. The total forested and total non-forested areas appear to be very similar in size.

To get an indication of possible uncertainties in the classification, the results from the corresponding rule files are analyzed. The rule files are raster files which show the probability for every pixel of being a member of a certain predefined class. In other words, in a rule file map it is calculated to which extent the spectral reflectance of each grid cell corresponds to the spectral reflectance of the

selected (ground-truth) end-member. Several training areas were created for each tree species, scattered over the map, and the statistics were calculated (table 4.6).

Table 4.6. The extents to which the spectral reflectance of the training areas of the five dominant species (columns) correspond to the spectral reflectance of the (ground-truth) end-members (rows). The less negative the rule-value, the higher the probability that the training areas of a certain species actually belongs to that species class.

	Abies alba	Fagus sylvatica	Picea abies	Quercus robur	Pinus sylvestris
Abies alba	***-28.6***	-35.5	-24.5	-26.6	-25.0
Fagus sylvatica	-59.0	***-22.3***	-23.5	-22.4	-25.7
Picea abies	-44.2	-41.7	***-20.5***	-23.4	-23.2
Quercus robur	-67.5	-37.6	-25.4	***-19.5***	-31.0
Pinus sylvestris	-53.8	-60.7	-25.6	-24.9	***-19.7***
Meadow	-141.1	-42.1	-57.6	-73.2	-102.6
Agr.crops	-371.4	-152.7	-97.6	-100.3	-60.2

In order to make the differences in table 4.6 more clear, the spectrally closest classes, meadows and agricultural crops, are included in the table. Considering for example the spectral reflectance of the *Abies alba* training areas, it appears that the correspondence of this spectral reflectance with the agricultural crop end-member spectral reflectance is very low (-371.4), compared to correspondence with the *Abies alba* end-member spectral reflectance (-28.6). From this table it becomes clear that the correspondence of the spectral reflectances of the *Abies alba* and *Fagus sylvatica* training areas to their end-member spectral reflectances are relatively high compared to the other end-member spectral reflectances. For the *Picea abies*, *Quercus robur* and *Pinus sylvestris*, these differences are less clear and therefore contain the highest classification uncertainty.

Keeping the abovementioned uncertainty in mind, the new developed species map is compared to the existing coarse species map from Land Vorarlberg (figure 2.4). First of all, the balance between forested and non-forested areas is very similar for both maps. Further, . the *Abies alba* or European silver fir is the most dominant species in the newly developed map, with a coverage of more than 25% of the total study area. However, the classification of Land Vorarlberg (2016) does not contain a separate class for the *Abies alba*, which makes it difficult to compare. The only method to compare the areas of the two maps covered by this species quantitatively is to sum the percentages of *Abies alba, Picea abies* and *Fagus sylvatica* coverage and compare this with the sum of the percentages of the *fir-spruce-beech, fir-spruce, beech* and *spruce* classes of Land Vorarlberg (2016). These sums are respectively 38.5% and 40.1% of the total study area, which seems to be comparable. Besides, almost all *Abies alba* dominated areas are situated within the same areas as the *fir-spruce-beech* and *fir-spruce* classes. However, it should be kept in mind that the *pioneer-afforestation* class of the Land Vorarlberg map can partly consist of one of these species, which would enlarge the sum of these species. Further, the latter *pioneer-afforestation* class has the highest diversity of species, which seems to be the case for the same areas in our own species map. Strikingly, the existing classification of Land Vorarlberg does not contain a class for the *Quercus robur* or *English oak*, while this is the second most common species in the newly developed classification map. Most parts of the new classification map which are classified as *Quercus robur* belong to the classes *pioneer-afforestation* or *beech* in the map of Land Vorarlberg. Finally, the portion of the forested area classified as *Pinus sylvestris* or Scots Pine is small in both maps. The most obvious mismatch between the two classification maps can be found in the northern and north-eastern part of the image. This is the area for which the 2012 flight date was on August 19, while the remaining part of the image was photographed in July 2012 (figure

3.4). This is also the part of the image which has a much higher elevation and contain steeper slopes, as the foothill of a mountain, than the remaining area, which lies within the valley between the mountains. Besides, for the north-eastern part of the image, it applies that the 2001 image also has a flight date which is three weeks later than the flight date of the rest of the image (figure 3.5). In the map of Land Vorarlberg this area has largely been classified as spruce or fir-spruce, while in the new map, next to the abundance of the oak in this area, all species occur in a scattering pattern.

4.2.2 Overall vegetation cover fraction map

When each grid cell was assigned to a certain class, the overall vegetation cover fractions were estimated using a relation between field-based canopy cover fractions and unmixing results of green vegetation. In figure 4.4, these field-based canopy cover fractions were plotted against the unmixing results for the same projected areas.

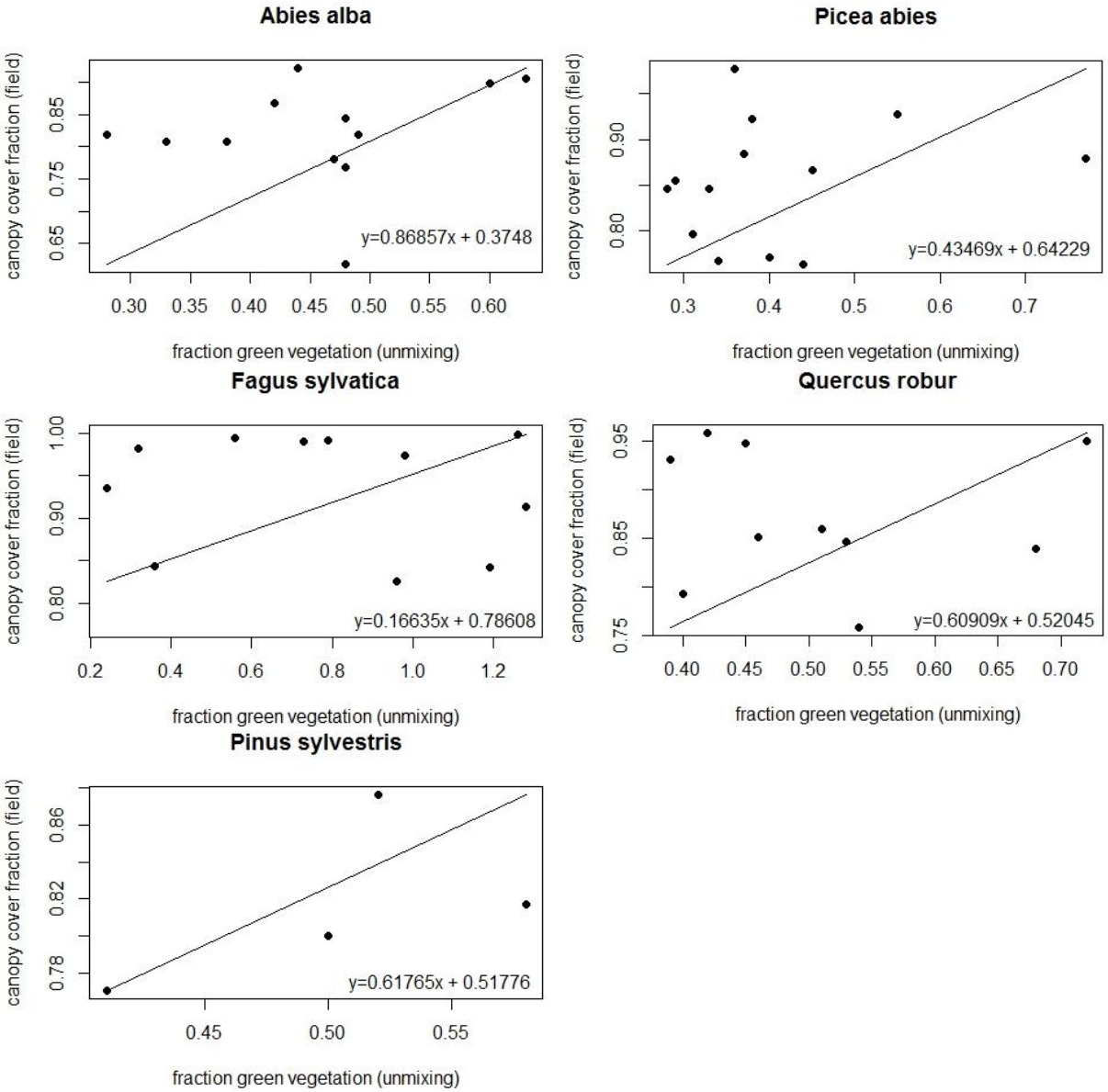

Figure 4.4. Field-derived canopy cover fractions plotted against the average fractions of green vegetation, derived by linear spectral unmixing. The straight lines and their corresponding equations represent the assumed relation between the two variables, based on the range of both the values from the field and the unmixing results.

As becomes clear from these plots, there is not a good correlation between the field measurements from 2015 and the computed green vegetation fractions on the basis of the RGB imagery of 2012. The field observation results of canopy cover fractions do have a narrow range compared to the unmixing results, and the fractions are generally high. However, because this method should theoretically work when the measurements were taken in the same period as the remote sensing imagery flight, it has been decided to use the results for the mapping of canopy cover fraction based on the following assumptions. We chose to assume that the range of field measurement results per species is a representative range for these species canopy cover fractions in the area (in the growing season). Besides, it is assumed that the range of plot average unmixing results per species is a representative range for plot average unmixing results per species in the image. Using these assumptions, straight lines are drawn in the plots that connect two imaginary points: one point which has the lowest value of unmixing results for that particular species plots as x value and the lowest value of c as y value, while the other point is located at the right top corner of the plot with the highest values for both as x- and y coordinates. One should not interpret these lines as regression lines, but as an upscaling method of the field measurements using the assumptions described above. The resulting c-map is created by converting the unmixing results into canopy cover fraction values using the equations given in the plots. This c-map is given in figure 4.5 and is displayed to a full A4 extent in Appendix B.

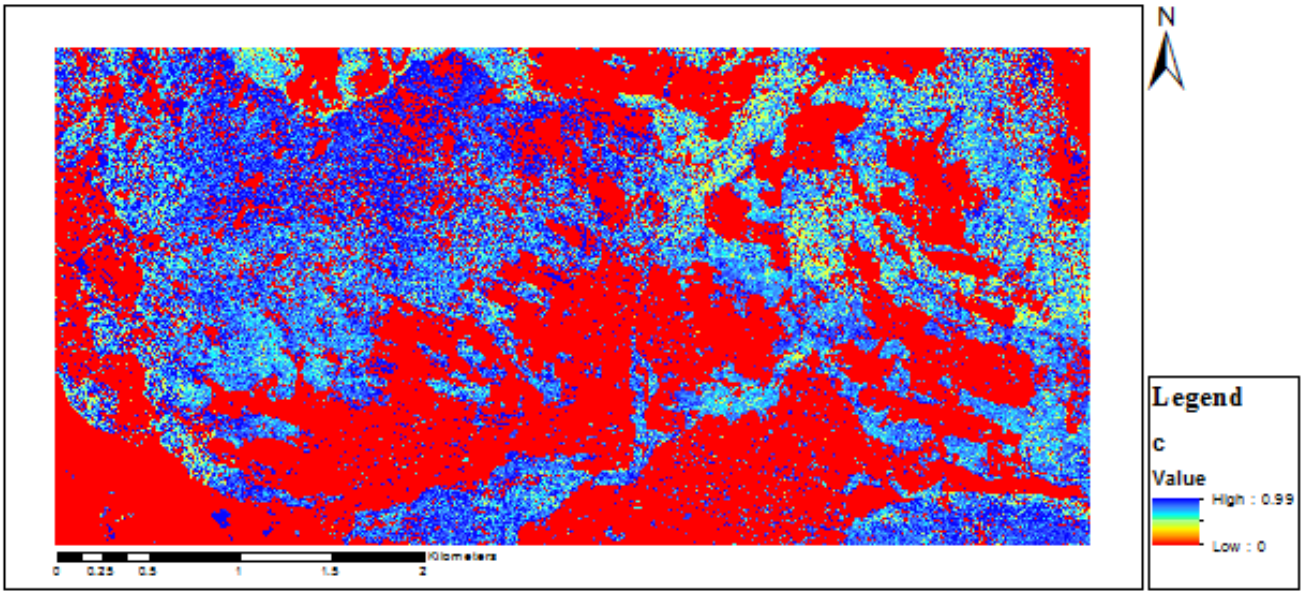

Figure 4.5. Overall vegetation cover fraction (c) map. Each grid cell contains a value for c between 0 (no vegetation cover) and 0.99 (highest vegetation cover).

The distributions of overall vegetation cover fractions per species in the map above are shown by area in figure 4.6.

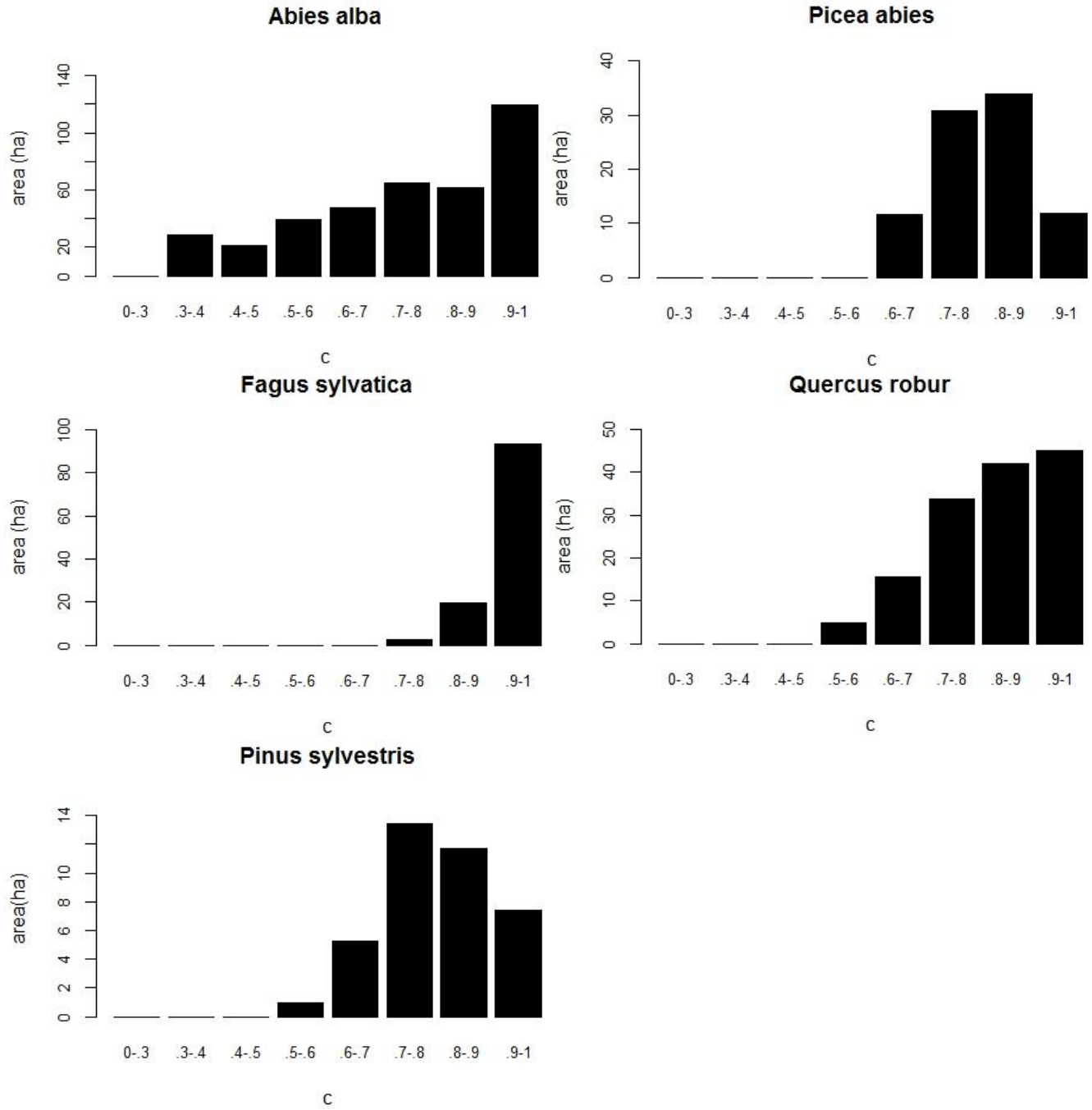

Figure 4.6. The distribution of c-values per species in the c-map by area. Note that the scales of the area-axis differ between each species.

4.2.3 Leaf Area Index map

The species specific LAI-canopy cover fraction relations which are presented in figure 4.2 were used for the conversion of the c-map into a LAI-map. The resulting map is presented in figure 4.7. A magnification of the map is presented in Appendix C.

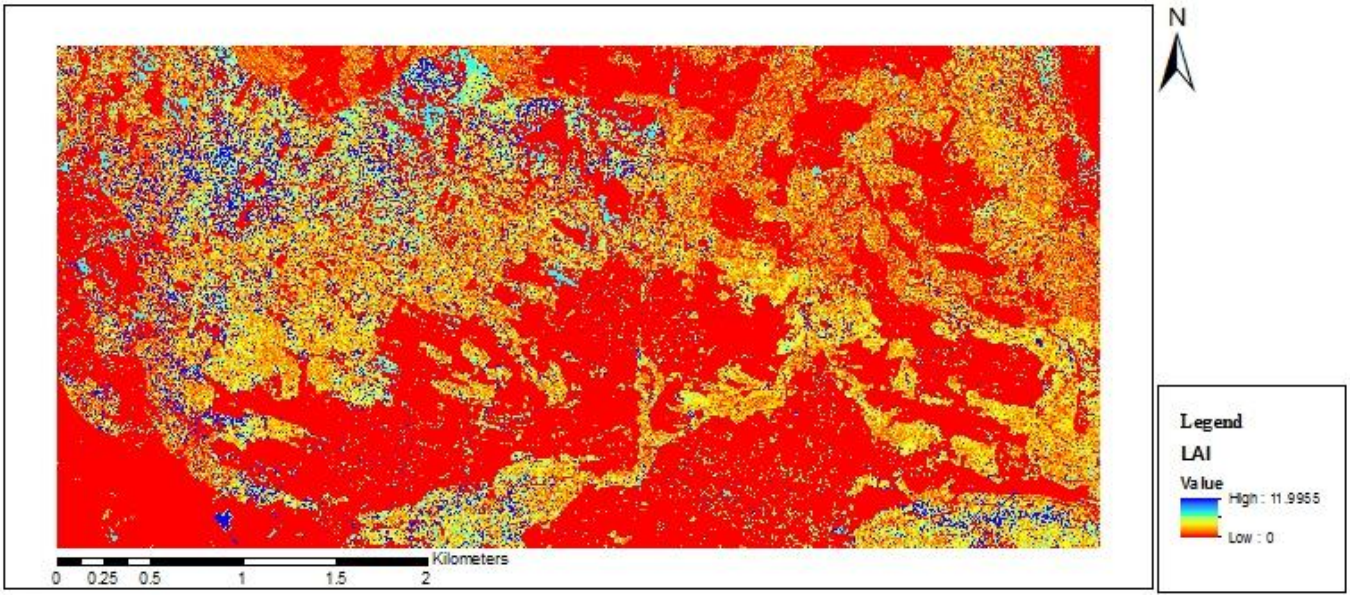

Figure 4.7. Leaf area index map. The LAI-values range between 0 and 12 m^2m^{-2} from red to blue. The calculations of LAI are based on the species-specific least-squares fitted Beer-Lambert equation and field observations.

The mean value of LAI in figure 4.7 is 4.6 m^2m^{-2}. An overview of the distribution of the LAI-values per species in the LAI map are presented by area in the bar charts below (figure 4.8).

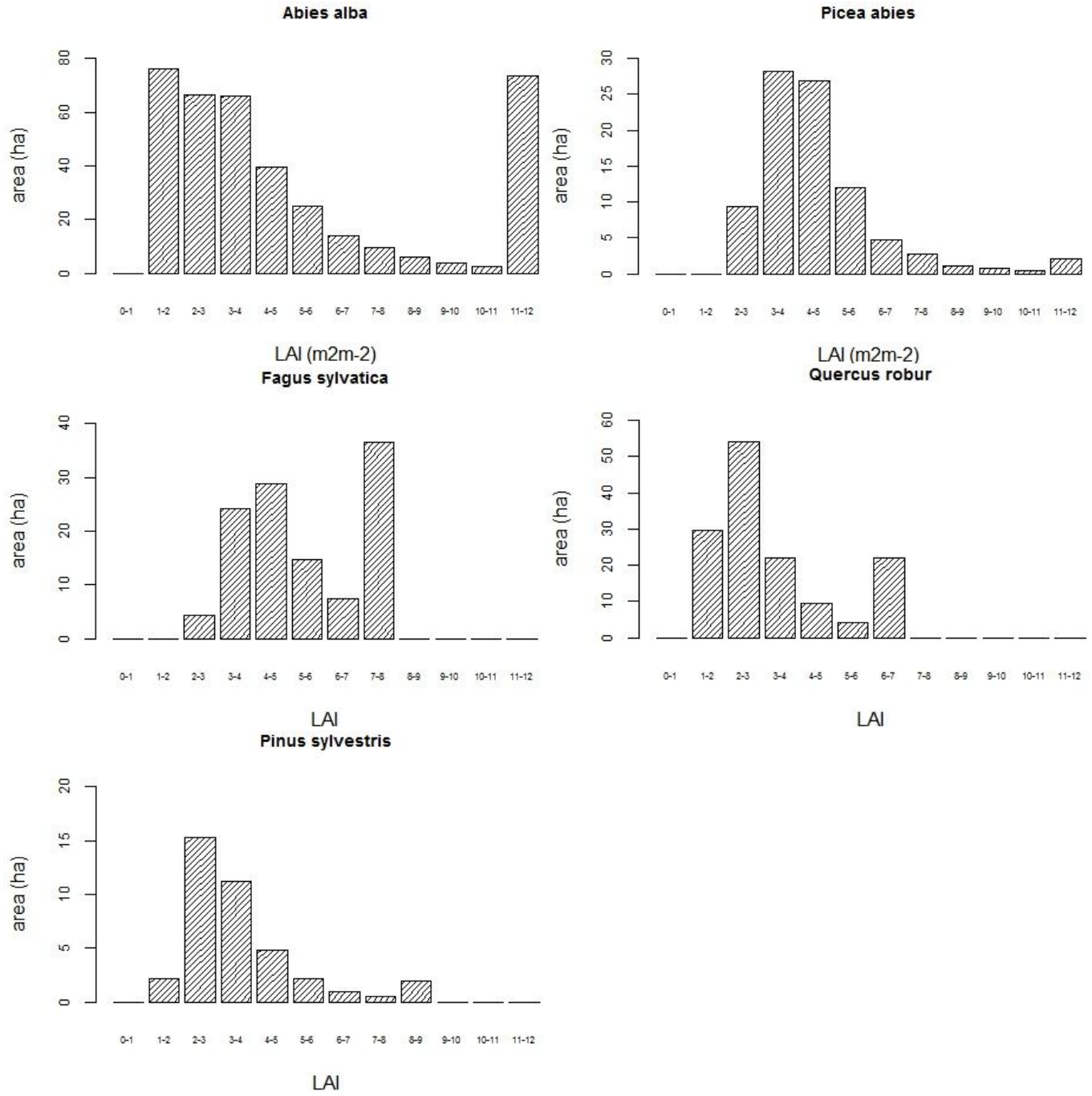

Figure 4.8. The distribution of LAI-values per species in the LAI-map by area. Note that the scales of the area-axis differ between each species.

4.2.4 Storage capacity map

Assuming that the species-specific field-based S_{max}-leaf area relations on branch-scale (figure 4.1) also exist on a grid cell scale (1 m^2), the LAI-map is converted into a S_{max}-map, using these relations. The resulting map is depicted in figure 4.9 and displayed to a larger extent in Appendix D.

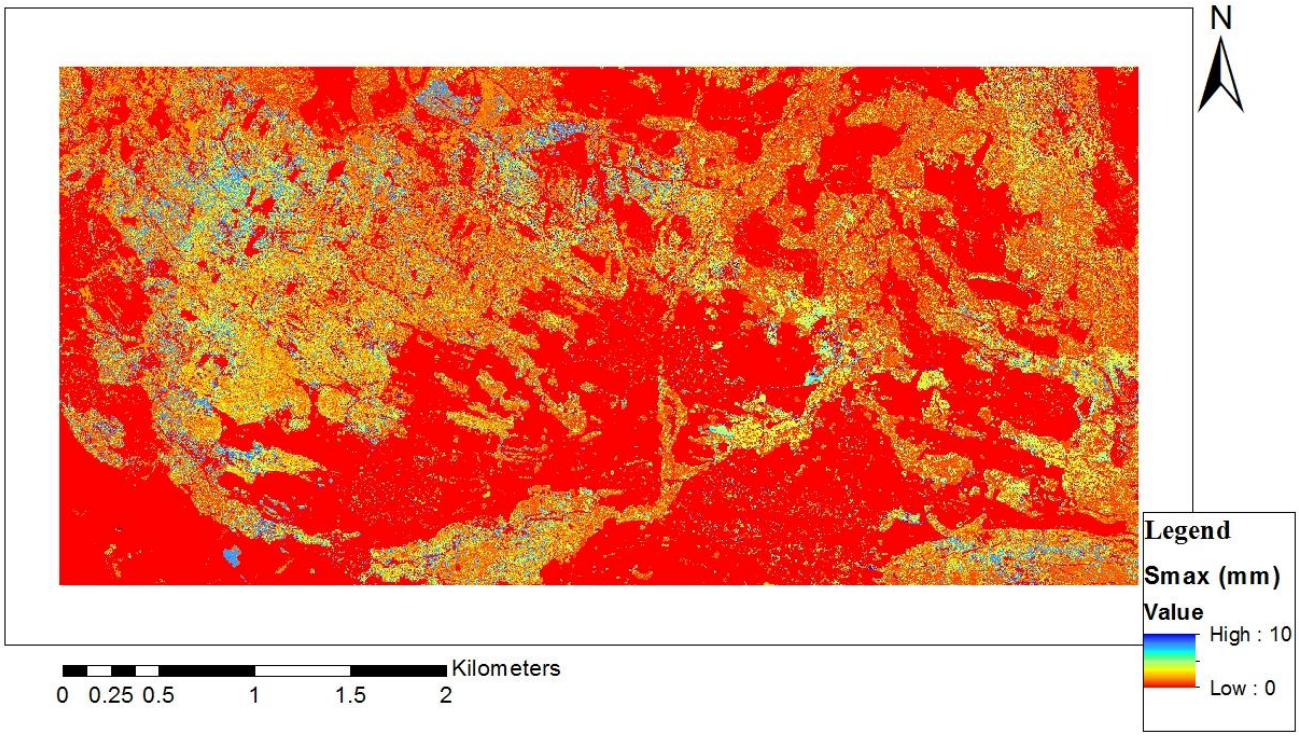

Figure 4.9. Maximum water storage (S_{max}) map. Each grid cell contains a S_{max} value between 0 (red) and 10.078 (blue) millimetres.

The S_{max}-map contains values between 0 and 10.078 mm. However, the low S_{max}-values are more common in the map, as becomes clear from the distribution of S_{max}-values per species in the S_{max}-map by area (figure 4.10). The mean value of S_{max} for a grid cell in the S_{max}-map is 2.3 mm. However, there are large differences in the distributions of S_{max}-values between the species.

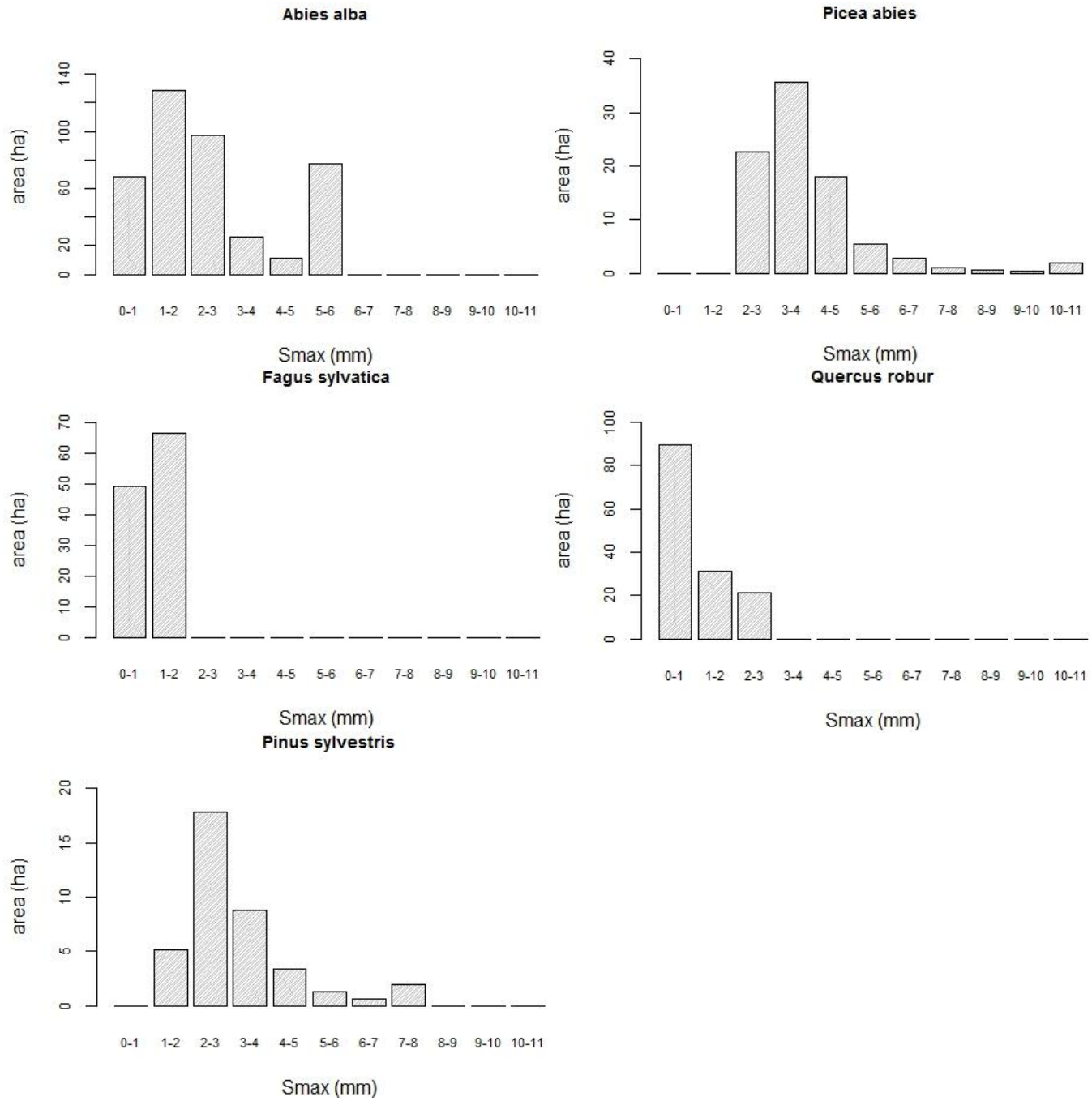

Figure 4.10. The distribution of S_{max}-values per species in the S_{max}-map by area. Note that the scales of the area-axis differ between each species.

Figure 4.10 shows that the S_{max}-values for the deciduous species (*Fagus sylvatica* and *Quercus robur*) in the S_{max}-map are generally much lower than the values for the coniferous species. For example, the highest S_{max}-values in the map for *Picea abies* classified grid cells (10.1 mm) are more than 6 times higher than the highest S_{max}-values in the map for *Fagus sylvatica* classified grid cells (1.6 mm). The mean S_{max}-values for grid cells classified with a deciduous species (both 1.1 mm) are between 2.4 to 3.5 times lower than the coniferous species classified grid cells: 2.6 mm (*Abies alba*), 3.2 mm (*Pinus sylvestris*) and 3.9 mm (*Picea abies*).

4.3 Interception model results

After the S_{max} values were mapped, an estimation of the canopy interception could be calculated and mapped using equation 5 and a certain input of gross precipitation. An example of a canopy interception map is given in figure 4.11. The amount of gross precipitation for this case is 20.2 mm, which is equal to one of the storm events measured during the fieldwork and will be discussed in the next paragraph. A magnification of figure 4.11 is presented in Appendix E.

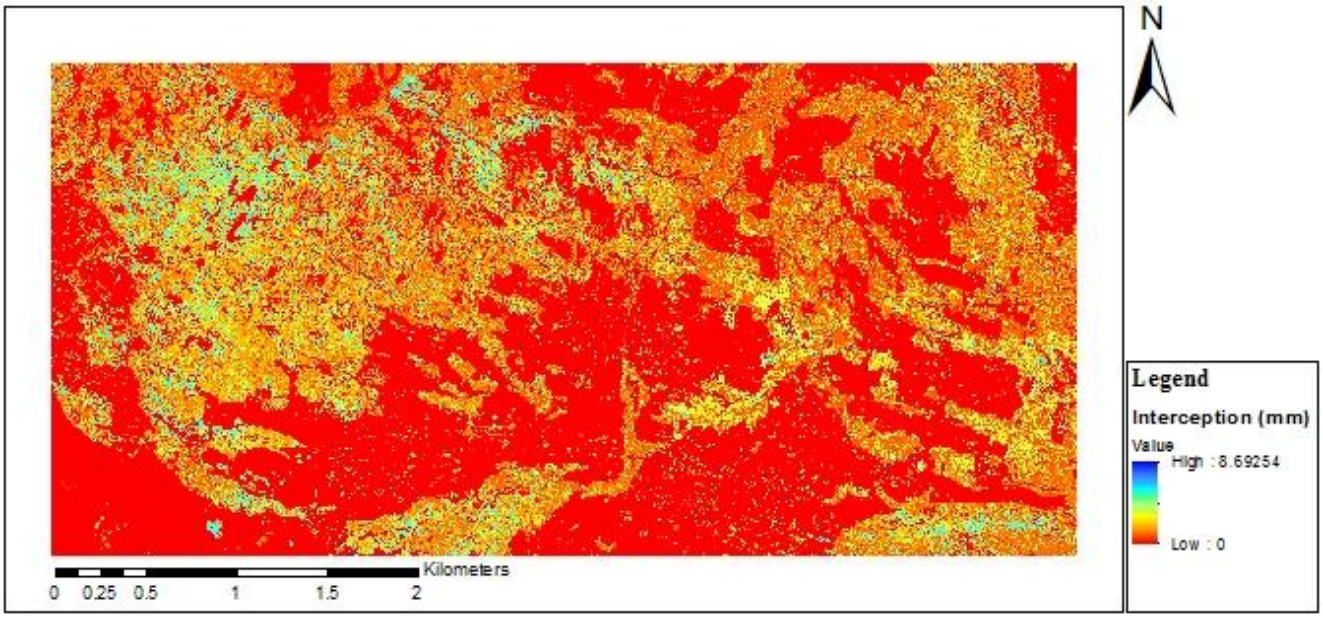

Figure 4.11. The mapped canopy interception for a gross precipitation amount of 20.2 mm. The interception values range between 0 (red) and 8.7 (blue) mm.

The fraction of gross precipitation that ends up as canopy interception is extremely dependent on the amount of gross precipitation. Figure 4.12 shows the species specific mean, minimum and maximum amounts of canopy interception for each amount of gross precipitation up to 40 mm, calculated by the model. Besides, the mean, minimum and maximum amounts of S_{max} per species are plotted in the graphs as straight horizontal lines.

Considering for example an average grid cell which is classified as *Abies alba*, which has a mean value for canopy cover fraction and a mean value for LAI. This grid cell intercepts more than 60% of the gross precipitation when the latter has an amount of 1 mm, assuming that no evaporation occurs during the storm event. However, this fraction decreases to 6.5% for a storm event of 40 mm and keeps decreasing for an increasing amount of rainfall. Since the assumption of no evaporation probably does not hold for a small event of 1mm, because the air around the leaves is expected to be not saturated for such small rainfall events, the model calculations are expected to be the most uncertain for the small rainfall events.

Furthermore, from these graphs it can be concluded that the modelled storage capacity (S_{max}) is reached for a much smaller amount of gross precipitation for an average deciduous classified grid cell (P is about 7 mm for a *Fagus sylvatica* and 11 mm for a *Quercus robur*) than for an average coniferous classified grid cell (P is about 21 mm for *Abies alba* and 35 mm for both *Picea abies* and *Pinus sylvestris*). However, these are results for grid cells with average characteristics for the particular species. The maximum storage capacity for the *Picea abies* grid cells with the highest cover and - LAI for example is not even reached with a gross precipitation of 40 mm.

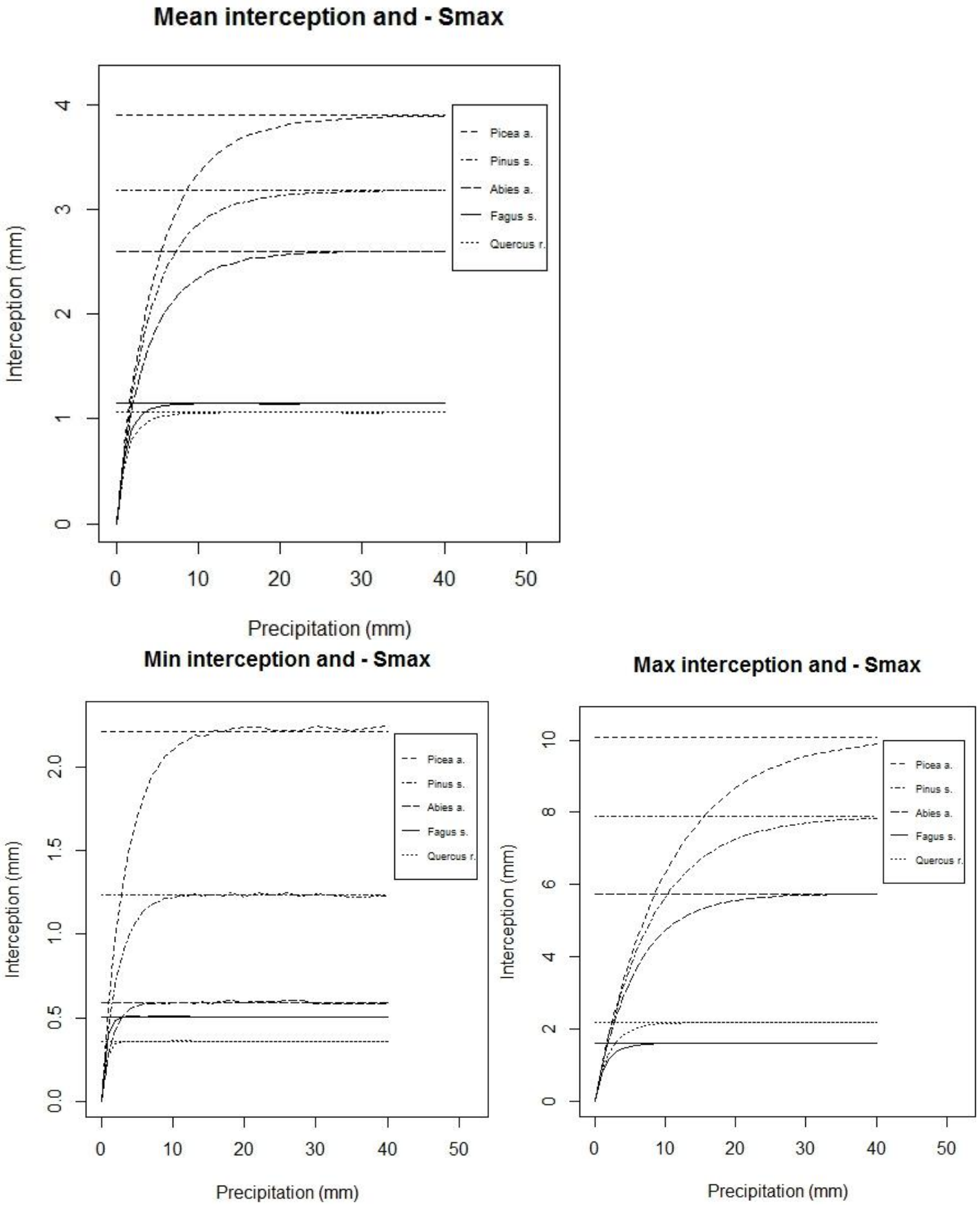

Figure 4.12. The mean, minimum and maximum model results for interception and S_{max} per species. The interception values are modelled for a range of input values of precipitation between 0 and 40 mm. The S_{max} values are given as straight horizontal lines.

5. Discussion

This study aimed at improving the spatial interception mapping approach presented by De Jong & Jetten (2007) by including relations between species-specific vegetation properties and interception. The influence of species-specific differences of leaf-and canopy structures on the interception process was studied on branch- and plot scale using measurements from the field. The fieldwork results were used to study the ability of a high-resolution remote sensing imagery based model to estimate the spatial variability of canopy interception on regional scale. Figures 4.11 and 4.12 show that it is possible to estimate this spatial variability of canopy interception on regional scale when species-specific vegetation properties are included in the model. However, in these figures, the validity of the developed methodology is not included. Therefore, this validity of the developed methodology is discussed in this chapter. In other words, this chapter serves as an overview to determine which parts of the methodology are well-developed and which parts could be improved.

The discussion is divided into five paragraphs, of which there are four that represent each a building block of the theoretical interception model which is used to map interception and is given in equation 5. Each paragraph gives an overview of the research uncertainties, gives an in-depth analysis of the results and compares the results of this study with results from other studies for that particular part of the model. The last paragraph discusses the final interception results and gives an analysis of the uncertainties in the final interception results.

5.1 Vegetation species mapping

A new vegetation species map was created using field observations and remote sensing data, because the existing classification map was too coarse for the purpose of this study. A supervised classification was applied using ground-truth data and the Maximum Likelihood Classifier method. Furthermore, a Majority Analysis was applied and the non-forested surface types were combined into one 'non-forest' class. This classification method is based on some assumptions and corresponding uncertainties. First of all, the vegetation classification is performed for the five dominant species in the study area, due to time limitations of the fieldwork period. These five species were selected based on the author's observations in the fieldwork area. However, these species do not cover 100% of the study area, while the resulting map gives the reader the impression that this is the case. It is the author's estimation that 70-80% of the study area is actually covered by the five selected species. Therefore, at least 20-30% is probably classified wrongly. Another major challenge in the classification process was the presence of a lot of shadow in the remote sensing images. The small shadows within the forest were partly removed by the enlargements of the grid cell size and the Majority Analysis. The larger shadows over open areas in the forest or over meadows were separately classified and eventually added to the non-forest class. However, a fraction of the shadowed grid cells remain misclassified becoming 'non-forest', while some grid cells might be covered with shaded understory vegetation. For these grid cells no interception is calculated.

Comparing the newly developed species map with the existing coarse species map from Land Vorarlberg (2016), it can be concluded that the classification of forests in general performed well, because the balance between forested and non-forested areas is very similar for both maps. When it comes to species classification, it can be concluded from the rule files results that the spectral differences between the species are small and this might lead to uncertainties in the classification. However, although the two species maps are broadly comparable when it comes to species occurrence, there are two main differences. The newly developed species map has a much higher resolution and is therefore the only one that is suitable for the purposes of this study. On the other hand, the species

map could be improved by selecting a broader range of species end-members for the classification. The map of Land Vorarlberg does cover a broader range of species.

More improvements on the current species classification could be made. For example, this classification might improve when the aerial photographs were taken on the same date. Also, when the NIR-band and the RGB-bands could have been collected from a dataset with the same flight date, instead of 11 years of time difference, the classification would theoretically improve significantly. This would also improve the assessment of the other model parameters. Besides, tree species classification using a Maximum Likelihood Classifier method is a relatively simple and common methodology, used by e.g. Martin *et al*. (1998). However, this classification could be improved significantly when an object-based approach was applied, instead of the current grid cell-based approach. An object-based classification approach is preferred over the current grid cell-based approach, because it theoretically overcomes the problem of salt-and-pepper effects usually found in grid cell-based classification (Yu *et al*., 2006). Unfortunately, this method is more time-consuming and could not be realized within the timeframe of this study. Also the challenge of dealing with the shaded grid cells might be improved using an alternative method. The grid cells which are classified as 'shadow' could be assigned to the spatially nearest classes using a method described in De Jong *et al*. (2001). This method first computes the Euclidean spectral distance in the feature space between the mean of every class in the end-member training set and the grid cell to be classified, and then accounts for the spatial information. However, this method requires more time than has been given for this study.

5.2 Assessment of the vegetation cover and leaf area index

Maps of overall canopy cover fraction and leaf are index were created as direct - and indirect input parameters for the exponential model. It was attempted to relate field measurements of canopy cover and LAI, acquired during a 3-week fieldwork period, to remote sensing products from 2012, to develop a c-map and a LAI-map. The c- and LAI values were estimated for 50 homogeneous plots using hemispherical photograph processing by the Can-EYE v6.314 software. Subsequently, the c- and LAI values were plotted per species and related using fitted Beer-Lambert equations. A c-map was created using a relation between the field measurements of canopy cover and the results of linear spectral unmixing of the 2012 RGB image. A LAI-map was eventually created using the species specific Beer-Lambert relations between the canopy cover and the LAI. This method is based on several assumptions and both the fieldwork as the image processing methodologies contain uncertainties.

First of all, the plots were selected on homogeneity in terms of tree species. However, since the selected circle of interest for the hemispherical photographs is 60°, a larger area is photographed than the plot size. Especially in relatively heterogeneous parts of the forest, other species with other characteristic leaf distributions influence the calculations of canopy cover and LAI. This can cause a significant error in the calculations by Can-EYE. Furthermore, Can-EYE calculates the LAI for six different approaches. Each approach is based on a different series of equations and assumptions. It appears that the resulting LAI calculations differ considerably between these approaches for a number of plots. Because the CEV5.1 approach resulted in, according to the author's estimate, the most reliable LAI estimations and this method's c - and LAI results had the best fit with the Beer-Lambert equation, the results from this approach were used. However, since the results have such a small similarity with the results from the other approaches, there might be a large uncertainty in especially the LAI estimation. Finally, the term 'leaf area index' actually does not fit to the Can-EYE image processing. The images were classified as partly 'sky' and partly 'vegetation'. However, these

'vegetation' class also contains stems, trunks and twigs. Hence, Can-EYE actually estimates the plant area index and the canopy cover including the woody parts of the plant. This could lead to a mismatch with the unmixing results, that are based on the 'green vegetation fractions'.

When we shift the focus from the fieldwork uncertainties to the uncertainties of the mapping of the overall canopy cover, the methodology can be discussed on several points. Figure 4.4 shows that there is not a good correlation between the canopy cover measurements from 2015 and the unmixing results from the RGB images from 2012. Since trees are extremely dynamic in leaf growth from year to year, especially the deciduous trees (e.g. Lowman, 1992), this mismatch lay within the expectations. Therefore, the ranges of canopy cover fractions per species were assumed to be representative ranges for the area as well as the ranges of unmixing results of green vegetation per species are representative ranges for the area. An artificial relation was created using these assumptions. This method should be considered as an approach to describe the spatial canopy cover variety. The relation between the field measurements and the unmixing results should theoretically be much better when the period of fieldwork was within the same period as the flight dates. The alternative method of this study described above gives vegetation cover fractions of 0.37 to 0.79, dependent on tree species, for unmixing fractions of green vegetation of 0. However, although small vegetation cover fractions are less abundant within the forests, it is expected that the largest uncertainties in the assessment of c-values can be found in the grid cells with a low unmixing value, while the high unmixing values contain the smallest error. The above mentioned relatively high y-axis intercepts of 0.37 to 0.79 result in high overall vegetation cover fractions in most vegetated grid cells in the image, which is presented in figure 4.6. Especially for the *Fagus sylvatica* and *Quercus robur* this seems to be a reasonably well approach during the growing season, when these species do have highly closed canopies. However, the relations between the unmixing results and the canopy cover fractions from the plot do not hold for the non-foliated season, where the canopy cover fractions should be around 0. Therefore, a larger range of canopy cover values is preferred over the current small range which is estimated from the hemispherical photographs, especially for the deciduous species. Since it is impossible to find low canopy cover fractions of *Fagus sylvatica* and *Quercus robur* during the growing season, field measurements should be taken during (the transition to) the non-foliated season.

Another major point of discussion is the manual cutting of the c-values at 0 and 1, since the vegetation cover fractions should have a value between 0 and 1. However, since the *1-fCover*-term in the Beer-Lambert law (equation 10) should be larger than 0, due to the nature of a natural logarithm, the fCover should be smaller than 1. Therefore, a maximum vegetation cover fraction of 0.99 is chosen for the c-map, assuming that at least 1% of a projected canopy is not covered by vegetation. This gives a reasonable range of LAI-values in the LAI-map (0-12), as can be seen in figure 4.7. However, because of the logarithmic character of the Beer-Lambert law, the estimation of LAI for highly dense canopies is extremely sensitive to the manually chosen maximum value of canopy cover fraction. A grid cell which is classified as *Fagus sylvatica* for example, can have a maximum LAI-value of 7.6 when the maximum vegetation cover fraction is established at 0.99. That maximum LAI-value will increase to 11.4 for a maximum vegetation cover fraction established at 0.999. Similarly, the maximum LAI-values of the *Abies alba* classified grid cells would increase from 11.0 to 16.5 respectively. From the per species distributions of c and LAI values presented in the figures 4.6 and 4.8 respectively, it becomes clear that this establishment of the maximum c-value is especially important for the two above mentioned species and hence contain the most uncertainties.

Taking the above mentioned uncertainties into account, the results from the c- and LAI maps are discussed and compared with previous published papers. As explained above, the canopy cover fractions determined from the hemispherical photographs have generally high values (0.618-0.999). In

the interception experiments from Aston (1979) however, a much broader range could be found (0.1-1). However, the canopy cover fractions in Aston(1979) are not measured, but should be seen as a model modification to get a reasonable model fit with the measurements. A better comparison could be made with other studies which measured canopy cover in the field such as Staelens *et al*. (2006), which measured a *Fagus sylvatica* canopy cover fraction of 0.81-0.997 with a mean of 0.94 in the growing season and 0.35-0.72 with a mean of 0.55 in the dormant season for 20 stands. This growing season range is very comparable with the canopy cover range of the 11 plots in this study, calculated by Can-EYE: 0.826-0.999. Furthermore, Llorens & Gallart (2000) found a canopy cover range of 0.63-0.87 for *Pinus sylvestris* stands, while the canopy covers of this species in this study had a range of 0.771-0.876. Finally, Korhoven *et al*. (2006) found canopy cover ranges of 0.51-0.89 for the *Picea abies* and 0.32-0.83 for the *Pinus sylvestris* for stand with tree heights larger than 7 meters. The results of these studies contribute to the reliability of the Can-EYE canopy cover calculations, the frequency distributions of c from figure 4.6 and especially the differences between the species.

Table 4.1 shows the extinction coefficients per species which are used to convert the c-map into a LAI map with the Beer-Lambert equation. These extinction coefficients are the result of solving the Beer-Lambert equation to the field measurement using the least-squares fit approach. The extinction coefficients from the deciduous species *Quercus robur* and *Fagus sylvatica*, 0.664 and 0.607 respectively, are clearly larger than those from the *Abies alba* and *Picea abies*, 0.418 and 0.384 respectively. Very comparable extinction coefficients can be found in other studies for the *Picea abies*. Bolstad & Gower (1990) for example find a *Picea abies* extinction coefficient of 0.39 for their fieldwork plots, while Bréda (2003) estimates extinction coefficients of 0.28-0.37 for the *Picea abies* stands in her study. In the same study of Bréda (2003) , extinction coefficients of 0.43-0.44 for the *Fagus sylvatica* stands and 0.31 for the *Abies sp*. stands are estimated. In most studies, the extinction coefficient values range generally from 0.3-0.7, with lower values for coniferous species and higher values for deciduous species (Marshall & Warring, 1986; Pierce & Running, 1988; Maass *et al*., 1995; Vose *et al*., 1995; Bréda, 2003). Therefore, using the extinction coefficients presented in table 4.1 to convert the c-map into a LAI-map might be considered as a reasonable approach.

Finally, figure 4.8 presents the frequency distribution of LAI-values in the LAI-map. Because most studies only give LAI values for single or a couple of plots, it is difficult to assess whether the LAI distributions of figure 4.8 are representative distributions for the specific species. However, most studies estimate LAI values between 5 and 7 for *Picea abies* plots (Lu *et al*., 1995; Johansson, 1999; Buchmann, 2000; Bréda, 2003; Lebourgeois, 2007), with some outliers with LAI values over 10 (Bolstad & Gower, 1990; Buchmann, 2000) or below 2 (Schume *et al*., 2003). The *Picea abies* classified grid cells in this study have LAI-values which range from 2.6 to 12 and have an average value of 4.6. The LAI of the *Abies alba* is much less studied, but Lebourgeois (2007) found for six *Abies alba* stands LAI values between 5.9 and 8.1. The grid cells in this study which are classified as *Abies alba* do have LAI values between 1.2 and 11.0, which is a much broader range. Also less studied is the LAI of *Fagus sylvatica* forest stands. Bréda (2003) for example finds a mean LAI value for several Fagus sylvatica stand of 5.4, while Meier & Leuschner (2008) estimate a LAI range of 5-9 based on numerous *Fagus sylvatica* plots with most LAI-values around 7. In the LAI map of this study the *Fagus sylvatica* LAI-values range from 2.4-7.6, with a mean of 5.4 and a large frequency of LAI values between 7 and 7.6. The mean LAI of the *Quercus sp.* is estimated by both Bréda (2003) and Gower *et al*. (1999) at around 4.4, which does not correspond with the mean LAI value of 3.4 for the *Quercus robur* found in this study. The results from the above mentioned studies imply that the LAI-map of this study could have a plausible range, but they can not determine whether the LAI values for the individual grid cells are estimated correctly.

To conclude, future studies that use comparable methodologies could obtain better results for a c- and LAI map with fewer uncertainties when the fieldwork period is within the same period as the flight date. This is because of the growth dynamics of trees. Besides, much better results are expected when a NIR-band is added to the RGB-bands. This is because the reflectance in the NIR-part of the spectrum is the highest for vegetation, which results theoretically into much better unmixing results for green vegetation. Finally, the top-right and top-center part of the image do contain the largest uncertainties in both the c- and LAI estimation, because of a different data acquisition date than the rest of the image. Therefore, the reflectance values differ from the calibrated relation between the unmixing results and the canopy cover from the field plots, which are all not located in this area. A study area which is entirely photographed at the same moment is therefore always preferred above the aerial photograph fragments of this study.

5.3 Conversion of LAI to S_{max}

The canopy storage capacity, S_{max}, is probably the most important factor in the exponential interception model. De Jong & Jetten (2007) showed that the S_{max} is directly related to leaf area and this relation is species-dependent. Because the species specific S_{max}-LAI relations have been barely studied for the dominant species in this study area, field measurements were required. The relations between S_{max} and leaf area were determined on branch-scale and used to convert the LAI-map into a S_{max}-map, assuming that the relations on branch-scale also hold for larger scales.

In this study, a very high artificial rainfall intensity is used to determine S_{max}. Following figure 4 from Aston (1979) the maximum water detention will be reached earlier when a higher rainfall intensity is used, but also the value of the maximum water detention will be slightly higher when a higher rainfall intensity is used. Therefore, the S_{max} values in this study might be overestimated when compared to real S_{max} values during real rainfall events. Besides, the storage capacity of the canopy in reality depends on the wind conditions during the rainfall event (Llorens & Gallart, 2000; Gerrits, 2010). Hence, the relations between S_{max} and leaf area presented in figure 4.1 only hold for very high precipitation amounts and windless conditions.

The leaf areas of the branches were estimated digitally using the color-differences between the branches and the white sheet in the photographs, combined with the knowledge of the photograph extents. However, not all branches had leaves or needles that were perfectly flat or did not overlap. Because of some overlap of the leaves or needles of especially the *Quercus robur*, *Pinus sylvestris* and *Picea abies*, some leaf areas could be underestimated. Finally, also for these branches it applies that actually the plant area was measured instead of the leaf area, because also the woody part of the branch is measured.

Despite of these small uncertainties, the resulting leaf areas and S_{max} values appear to have relatively high correlations. For each unit increase of leaf area, the *Picea abies* and the *Pinus sylvestris* detain the largest volumes of water, while the *Fagus sylvatica* and the *Quercus robur* detain the smallest amount of water. This difference in water detention is confirmed by Parker (1995) and can simply be attributed to their leaf - or needle structure. The needles of the *Picea abies* and *Pinus sylvestris* are structured around the twig in such a way that water droplets can be easily detained. The needles of the *Abies alba* are relatively flat with respect to the twig and besides are somewhat smoother than the other coniferous species. Therefore water can less easily be detained. The large, smooth leaf surfaces of the deciduous species at last are the least efficient when it comes to water detention.

Although S_{max}-LAI relations have been little studied, the present S_{max}-LAI relations from different studies are summarized by De Jong & Jetten (2007) and separated by conifers, broadleaved trees and

shrubs and grasses. Because little data is available, some species are combined in order to find a relation. From these figures it appears that the broadleaved Olive tree detains water droplets easier than coniferous spruce and pine species. This contrasts with the results from this study. However, the structure of the Olive tree is very different from the structure of the *Fagus sylvatica* and *Quercus robur* and hence cannot be compared.

When the trend line of the combined pine species from figure 3 in De Jong & Jetten (2007) is compared to the S_{max}- leaf area relation found in this study, a striking difference can be found. When for example the S_{max} is calculated for both relations using a LAI of 4, the pine species relation gives a S_{max} of 1 mm, while the relation in figure 4.1 gives a S_{max} of 3.5 mm.

This might be due to the fact that a other rainfall intensities were used in the studies. Following the previous mentioned figure 4 of Aston (1979), the S_{max} increases for higher rainfall intensities. This could be an explanation for the higher S_{max} in this study. Another explanation could be that the other pine species, which results are included in the relation, can detain much less water than the *Pinus sylvestris*. A third explanation for the non-similarity could be that the S_{max}- leaf area relations found on branch scale do not hold for larger scale plots.

The relations between S_{max} and leaf area found in this study were used to create a S_{max}-map, shown in figure 4.9. From the frequency distributions of S_{max}, presented in figure 4.10, it appears that almost 60% of the forested grid cells contain S_{max} values between 0 and 2 and 98.8% of all forested grid cells contain S_{max} values between 0 and 6 mm. The S_{max} range of the deciduous species in the S_{max}-map seem to broadly coincide with the broadleaved rain forest S_{max} range of figure 3 in De Jong & Jetten (2007). However, the coniferous S_{max} ranges do not coincide, since the model generally estimates higher S_{max} values. Parker (1995) estimates a general interception capacity range between 1 and 3 mm, which coincides with the largest part of this S_{max} map.

To conclude, definitely more research needs to be done on the relation between S_{max} and LAI for different species, because it is difficult to assess whether the model estimates reasonable values for S_{max}. It is uncertain whether the branch-scale measurements also hold for large-scale areas. The S_{max} values found in this study are probably overestimated compared to reality due to the high rainfall intensities during the experiments. Also more research should be done on the influence of wind on the S_{max}.

5.4 Interception

The aim of this research was to improve the remote sensing approach of quantitatively mapping canopy interception , described in De Jong & Jetten (2007), by using species-specific relations from the field. The vegetation characteristics described in the paragraphs above were used as input variables for the exponential model, which in turn is used to assess the canopy interception per grid cell for a given amount of precipitation. Finally, the exponential model performance was tested on plot-scale, using the results from field experiments.

The exponential model estimates an interception on storm event-basis, thereby assuming a negligible influence of evaporation. This assumption is the most reliable for large storm events. Besides, the relations between S_{max} and leaf area were determined for high intensity storms, without any influence of wind and with initially dry leaves. Therefore, it is expected that the model performs best for windless large rainfall events with high intensities after initial dry conditions of the canopy. Besides, the model does only work for the growing season, as explained in the previous paragraphs, and does not take snowfall into account.

Especially the assumption of initial dry conditions and the exclusion of snowfall in the model could be problematic for this mountainous study region. The northern and north-eastern part of the study area is characterized by a high elevation and therefore might be covered by snow for a considerable part of the year. Besides, during the fieldwork period the area was covered by low clouds a couple of times, which wetted the leaves considerably. If this is a common phenomenon in this area, the assumption of an initial dry situation might not hold so often and the percentage of precipitation which is intercepted by the canopy might be lower than the resulting model estimations.

The performance of the exponential model was tested with interception measurements in three plots in the study area. Unfortunately, there were only three rainfall events during the fieldwork period, which makes the calibration of the model using these field experiments very uncertain. Therefore, it has been chosen not to calibrate the model with the field experiment results, but rather regard them as performance tests. The interception of two *Picea abies* plots and one *Fagus sylvatica* plot have been measured, using simple rain gauges inside the plots to measure throughfall and outside the plots to measure gross precipitation. Stemflow was assumed to be negligible, because of the general low values of stemflow found in literature, the relative low accuracy of the throughfall - and gross precipitation measurements and the difficult - and time-consuming character of stemflow measurements. Hence, an initial (small) error is expected due to the neglecting of stemflow.

In order to judge whether the model performs well, it would have been better to measure throughfall for all five dominant species, especially for at least one *Abies alba* plot, which is the most common species in the study area. However, in the fieldwork area the *Picea abies* was by far the most common species. During the fieldwork period, it was yet unknown that the *Abies alba* would be the dominant species in the entire study area. Besides, homogeneous *Abies alba* plots were first found in the last week of the fieldwork period. Hence, because of these reasons and because of a limited amount of rain gauges, two *Picea abies* plots and one *Fagus sylvatica* plot have been measured.

In most cases, the field measurements of interception did not coincide with the exponential model calculations for the same plots. In all cases, the exponential model underestimated the canopy interception, with the most extreme underestimation for the *Fagus sylvatica* plot. This disagreement could have been caused by multiple reasons. First, the LAI for the plots could be underestimated by Can-EYE. This hypothesis is tested by calculating the best-fit LAI-values for the interception measurements of the 20.2 mm storm event with the Beer-Lambert law. Since the best-fit LAI for the *Fagus sylvatica* was extremely high (24.7 m^2m^{-2}) and the corresponding extinction coefficient was extremely low (0.111), this hypothesis is not likely for the *Fagus sylvatica*. On the other hand, fitting the LAI and extinction coefficients for the *Picea abies* plots gave reasonable results: 8.7 and 0.303 for plot 2 and 4.0 and 0.366 for plot 3 respectively. Second, the relations between S_{max} and leaf area simply might not hold for larger scales. This hypothesis could not be tested within the scope of this study. Last, the exponential model simply does not perform well for especially *Fagus sylvatica* stands in the field. Since the second and the last hypothesis can not be excluded or confirmed using so little field data, clearly more research needs to be done.

Figure 4.12 presents the species specific mean, maximum and minimum interception values for gross precipitation values between 0 and 40 mm. It shows that the maximum storage capacity for the deciduous species is reached for a much smaller storm than for the coniferous species. It also shows that the fraction of precipitation which is intercepted is extremely dependent on the amount of precipitation, using this approach. This coincides for example with Gómez *et al*. (2001), who plotted the fraction of precipitation which ends up as interception against the gross precipitation for Olive trees, and is confirmed by Crockford & Richardson (2000). The figure also shows that for a large

rainfall event (P>20 mm), the coniferous classified grid cells in the model have a mean canopy interception value of 2.5-4 mm, while the deciduous classified grid cells have a mean canopy interception value of about 1.1 mm. Because canopy interception is dependent on LAI, canopy coverage, species and weather conditions it is difficult to compare the values of canopy interception from other papers, partly presented in the introduction, to the values modelled for this study region.

6. Conclusion and recommendations

6.1 Conclusions

This study focused on the ability to quantitatively estimate the spatial variability of canopy interception on regional scale. The aim of this study was to improve the spatial interception mapping approach developed by De Jong & Jetten (2007), by including relations between species-specific vegetation properties and interception. A two-fold methodology was applied to achieve this goal. First, the influence of species-specific differences of leaf- and canopy structures on the interception process was studied. In a study region in Vorarlberg (Austria) fieldwork was performed on branch- and plot scale in order to find relations between these vegetation properties and the interception process. Second, it was studied whether these species-specific differences could be implemented in a high-resolution remote sensing imagery based model to estimate the spatial variability of canopy interception on regional scale.

Promising fieldwork results both on branch- and plot- scale contributed to the understanding of the relation between species-specific vegetation properties and interception. Clear relations between leaf area and storage capacity were found for different species, which can be attributed to the species-specific leaf- and branch structures. It appears that the coniferous species hold water much better for the same leaf area than the deciduous species. On plot-scale, relations between canopy cover fractions and leaf area indexes for different species were assessed, which were useful as converting tools for the model.

Besides, the usage of high-resolution imagery contributed to an increase in spatially detail in the variability of vegetation species cover, canopy cover, leaf area index, storage capacity and eventually interception estimation. Therefore, it is concluded that the results of this study contributed to an improvement of the current approach of quantitatively estimate the spatial variability of canopy interception developed by De Jong & Jetten (2007).

However, the approach still contains several uncertainties. The largest uncertainty is probably the assessment of the overall vegetation cover fraction using both field estimations of canopy cover fraction and linear spectral unmixing results. Because no correlation was found between the field estimations and the remote sensing products, an artificial relation was used which was based on several assumptions and uncertainties. Because the overall vegetation cover fraction map does not only serve as a direct input variable of the model, but also indirectly determines the LAI and storage capacity maps, uncertainties in this estimations have major effects on the entire interception model. Besides, due to the logarithmic character of the Beer-Lambert equation, the LAI assessment is extremely sensitive to small errors in the overall canopy cover fraction, especially for high cover fractions. Therefore, major improvements can be made when these uncertainties are minimized.

The second largest uncertainty is presumably caused by the lack of interception measurements on plot-scale. Therefore, the model could not be calibrated by field measurements. Accurate calibration could largely improve the estimation of interception by the model.

Thirdly, the remote sensing imagery consisted of aerial photographs which had different acquisition dates. This makes that the northern - and north-eastern part of the study area have probably less reliable interception estimations than the remaining area.

Furthermore, there were some fieldwork uncertainties. The branch-scale storage capacity is probably slightly overestimated due to the usage of extremely high rainfall simulations. This could lead to an overestimation of the interception in the model. Besides, it is uncertain whether the relations between leaf area and storage capacity on branch-scale also hold for larger scales, as is assumed in this study.

Another fieldwork uncertainty is the assessment of LAI values using hemispherical photograph analysis. The different methodologies used by Can-EYE give divergent LAI values for the same set of photographs. This implies that this analysis is hard and uncertainties should be taken into account.

Finally, the vegetation species map used for the analysis only contains five species, while more species occur in the area, each with its own specific relations with rainfall interception. However, because from the comparison with the species map of Land Vorarlberg it seems that especially non-included deciduous species should replace parts of the included deciduous classified areas, the influence of this possible misclassification on the interception is not that large. After all, the difference in interception between the deciduous species turned out to be smaller than the difference between deciduous and coniferous species.

6.2 Recommendations

To improve the developed methodology, several recommendations are given for future research in this field. To minimize the largest uncertainty given above, it is recommended to do plan the fieldwork in the same period as the airborne data acquisition. Because vegetation is extremely variable in time, the differences between the remote sensing products and the fieldwork could be minimized when these conditions are met, and this would theoretically largely improve the results.

Second, since the LAI estimations are based on the Beer-Lambert equations, the model is very sensitive to the extinction coefficients. More fieldwork experiments, especially interception measurements, would theoretically largely improve the model results, because the model could be calibrated with field measurements. In the summer months, large storm events with high rainfall intensities are expected to occur regularly. Besides, high evaporation rates between the storm events dry the leaves, which is an initial assumption for the model. Therefore, the interception measurements can best be performed during the summer months. However, when it is aimed that the model can also estimate temporal patterns of canopy interception, a broad range of canopy cover fractions and LAI values is required, and therefore fieldwork should also be performed during the dormant season and during the transition from growing to dormant season.

Besides, a remote sensing imagery dataset which includes more spectral bands, especially in the NIR region, should improve the remote sensing products which were used for analysis. In the NIR region of the electromagnetic spectrum, green vegetation has the highest reflection, which makes this the most interesting region for spectral unmixing in order to estimate vegetation cover fractions. Besides, the largest differences between vegetation species can be observed, which improves the classification.

For the species classification, in general it applies that the more species could be measured, the smaller the uncertainty in the classification. Besides, classification improvements could be made using other methodologies such as object-based classification and a more sophisticated approach to deal with shadows, which is described by De Jong *et al.* (2001). However, it should be taken into account that these methodologies are more time-consuming.

Finally, it is uncertain whether the relations between the storage capacity and leaf area on branch-scale also hold for larger scales. More research should be done in this field to make the results more reliable.

Bibliography

Álvarez, F., Catanzarite, T., Rodriguez-Perez, J. E., & Nafria, D. (2010). Radiometric Calibration and Evaluation of Ultracam X and Xp Using Portable Reflectance Targets and Spectrometer Data. Application to Extract Thematic Data from Imagery Gathered by the National Plan of Aerial Orthophotography (PNOA). In: *International Calibration and Orientation Workshop*. Spain: Castelldefels.

Amann, G., Schennach R., Kessler J., Maier B., & Terzer S. (2014). *Handbuch der Vorarlberger Waldgesellschaften: Gesellschaftsbeschreibungen und waldbaulicher Leitfaden*. Dornbirn: Buch & Offsetdruck Verlag Hugo Mayer GmbH.

Anzhi, W., Jinzhong, L., Jianmei, L., Tiefan, P., & Changjie, J. (2005). A semi-theoretical model of canopy rainfall interception for Pinus koraiensis nakai. *Ecological Modelling*, *184*(2), 355-361.

Asdak, C., Jarvis, P. G., Van Gardingen, P., & Fraser, A. (1998). Rainfall interception loss in unlogged and logged forest areas of Central Kalimantan, Indonesia. *Journal of Hydrology*, *206*(3), 237-244.

Aston, A. R. (1979). Rainfall interception by eight small trees. *Journal of hydrology*, *42*(3), 383-396.

Bolstad, P. V., & Gower, S. T. (1990). Estimation of leaf area index in fourteen southern Wisconsin forest stands using a portable radiometer. *Tree physiology*,*7*(1-2-3-4), 115-124.

Bréda, N. J. (2003). Ground-based measurements of leaf area index: a review of methods, instruments and current controversies. *Journal of experimental botany*, *54*(392), 2403-2417.

Buchmann, N. (2000). Biotic and abiotic factors controlling soil respiration rates in Picea abies stands. *Soil Biology and Biochemistry*, *32*(11), 1625-1635.

Bulcock, H. H., & Jewitt, G. P. W. (2010). Spatial mapping of leaf area index using hyperspectral remote sensing for hydrological applications with a particular focus on canopy interception. *Hydrology and Earth System Sciences*,*14*(2), 383-392.

Chen, J.M., Rich, P.M., Gower, S.T., Norman, J.M., & Plummer, S. (1997). Leaf area index of boreal forests: Theory, techniques and measurements. *Journal of Geophysical Research, 102*(24), 29429-29443.

Crockford, R. H., & Richardson, D. P. (2000). Partitioning of rainfall into throughfall, stemflow and interception: effect of forest type, ground cover and climate. *Hydrological processes*, *14*(16-17), 2903-2920.

De Jong, S. M., Hornstra, T., & Maas, H. G. (2001). An integrated spatial and spectral approach to the classification of Mediterranean land cover types: the SSC method. *International Journal of Applied Earth Observation and Geoinformation*, *3*(2), 176-183.

De Jong, S. M., & Jetten, V. G. (2007). Estimating spatial patterns of rainfall interception from remotely sensed vegetation indices and spectral mixture analysis. *International Journal of Geographical Information Science*, *21*(5), 529-545.

Dunne, T., & Leopold, L.B. (1978). *Water in Environmental Planning* . New York: W.H. Freeman & Company.

Gerrits, A. M. J. (2010). *The role of interception in the hydrological cycle*. PhD dissertation. Delft University of Technology, The Netherlands.

Gerrits, A. M. J., Pfister, L., & Savenije, H. H. G. (2010). Spatial and temporal variability of canopy and forest floor interception in a beech forest. *Hydrological processes*, *24*(21), 3011-3025.

Gómez, J. A., Giráldez, J. V., & Fereres, E. (2001). Rainfall interception by olive trees in relation to leaf area. *Agricultural Water Management*, *49*(1), 65-76.

Gould, W. (2000). Remote sensing of vegetation, plant species richness, and regional biodiversity hotspots. *Ecological applications*, *10*(6), 1861-1870.

Helvey, J., & Patric, J. H. (1965). Canopy and litter interception of rainfall by hardwoods of eastern United States. *Water Resources Research*, *1*(2), 193-206.

Herbst, M., Roberts, J. M., Rosier, P. T., & Gowing, D. J. (2006). Measuring and modelling the rainfall interception loss by hedgerows in southern England. *Agricultural and Forest Meteorology*, *141*(2), 244-256.

Herwitz, S. R. (1985). Interception storage capacities of tropical rainforest canopy trees. *Journal of Hydrology*, *77*(1-4), 237-252.

Horton, R. E. (1919). Rainfall interception. *Monthly weather review*, *47*(9), 603-623.

Hutjes, R. W. A., Wierda, A., & Veen, A. W. L. (1990). Rainfall interception in the Tai Forest, Ivory Coast: application of two simulation models to a humid tropical system. *Journal of Hydrology*, *114*(3), 259-275.

Johansson, T. (1999). Biomass production of Norway spruce (Picea abies (L.) Karst.) growing on abandoned farmland. *Silva Fennica*, *33*(4), 261-280.

Jonckheere, I., Fleck, S., Nackaerts, K., Muys, B., Coppin, P., Weiss, M., & Baret, F. (2004). Review of methods for in situ leaf area index determination: Part I. Theories, sensors and hemispherical photography. *Agricultural and forest meteorology*, *121*(1), 19-35.

Karssenberg, D. (2014). *PCRaster 4.0.2 software*. Received on 12-12-2015 from <<http://pcraster.geo.uu.nl/pcraster-4-0-2/>>

Kelliher, F. M., Whitehead, D., & Pollock, D. S. (1992). Rainfall interception by trees and slash in a young Pinus radiata D. Don stand. *Journal of Hydrology*,*131*(1-4), 187-204.

Land Vorarlberg (2016). *VoGIS Geodaten*. Received on 6-1-2016 from <<http://vogis.cnv.at>>

Lankreijer, H., Lundberg, A., Grelle, A., Lindroth, A., & Seibert, J. (1999). Evaporation and storage of intercepted rain analysed by comparing two models applied to a boreal forest. *Agricultural and Forest Meteorology*, *98*, 595-604.

Lebourgeois, F. (2007). Climatic signal in annual growth variation of silver fir (Abies alba Mill.) and spruce (Picea abies Karst.) from the French Permanent Plot Network (RENECOFOR). *Annals of Forest Science*, *64*(3), 333-343.

Leuzinger, S., & Körner, C. (2007). Tree species diversity affects canopy leaf temperatures in a mature temperate forest. *Agricultural and Forest Meteorology*, *146*(1), 29-37.

Lindenmaier, F., Zehe, E., Wienhöfer, J., & Ihringer, J. (2008). Hydrological patterns and processes of a deep seated creeping slope at Ebnit, Vorarlberg. In: *Interpraevent 2008, conference proceedings, 2*, 183-194.

Linsley, R. K., Kohler, M. A., & Paulhus, J. L. (1949). *Applied Hydrology*, New York: McGraw-Hill Book Company.

Liu, S. (1997). A new model for the prediction of rainfall interception in forest canopies. *Ecological Modelling*, *99*(2), 151-159.

Llorens, P., & Gallart, F. (2000). A simplified method for forest water storage capacity measurement. *Journal of Hydrology*, *240*(1), 131-144.

Llorens, P., Poch, R., Latron, J., & Gallart, F. (1997). Rainfall interception by a Pinus sylvestris forest patch overgrown in a Mediterranean mountainous abandoned area I. Monitoring design and results down to the event scale. *Journal of hydrology*, *199*(3), 331-345.

Lloyd, C. R., Gash, J. H. C., & Shuttleworth, W. J. (1988). The measurement and modelling of rainfall interception by Amazonian rain forest. *Agricultural and Forest Meteorology*, *43*(3), 277-294.

Lowman, M. D. (1992). Leaf growth dynamics and herbivory in five species of Australian rain-forest canopy trees. *Journal of Ecology*, 433-447.

Lu, P., Biron, P., Bréda, N., & Granier, A. (1995). Water relations of adult Norway spruce (Picea abies (L) Karst) under soil drought in the Vosges mountains: water potential, stomatal conductance and transpiration. In *Annales Des Sciences Forestieres*, *52*(2), 117-129.

Lull, H. W., & Sopper, W. E. (1969). Hydrologic effects from urbanization of forested watersheds in the Northeast. *USDA Forest Service Research Paper NE-146*, 1-31.

Maass, J., Vose, J. M., Swank, W. T., & Martínez-Yrízar, A. (1995). Seasonal changes of leaf area index (LAI) in a tropical deciduous forest in west Mexico. *Forest Ecology and Management*, *74*(1), 171-180.

Macfarlane, C., Hoffman, M., Eamus, D., Kerp, N., Higginson, S., McMurtrie, R., & Adams, M. (2007). Estimation of leaf area index in eucalypt forest using digital photography. *Agricultural and Forest Meteorology*, *143*(3), 176-188.

Markart, G., Perzl, F., Kohl, B., Luzian, R., Kleemayr, K., Ess, B., & Mayerl, J. (2007). *22. und 23. August 2005-Analyse von Hochwasser-und Rutschungsereignisse in ausgewählten Gemeinden Vorarlbergs*. Innsbruck: Bundesforschungs- und Aubildungszentrum für Wald, Naturgefahren und Landschaft.

Marshall, J. D., & Waring, R. H. (1986). Comparison of methods of estimating leaf-area index in old-growth Douglas-fir. *Ecology*, *67*(4), 975-979.

Martens, S. N., Ustin, S. L., & Rousseau, R. A. (1993). Estimation of tree canopy leaf area index by gap fraction analysis. *Forest Ecology and Management*, *61*(1), 91-108.

Martin, M. E., Newman, S. D., Aber, J. D., & Congalton, R. G. (1998). Determining forest species composition using high spectral resolution remote sensing data. *Remote Sensing of Environment*, *65*(3), 249-254.

Meier, I. C., & Leuschner, C. (2008). Leaf size and leaf area index in Fagus sylvatica forests: competing effects of precipitation, temperature, and nitrogen availability. *Ecosystems*, *11*(5), 655-669.

Merriam, R. A. (1960). A note on the interception loss equation. *Journal of Geophysical Research*, *65*(11), 3850-3851.

Morsdorf, F., Kötz, B., Meier, E., Itten, K. I., & Allgöwer, B. (2006). Estimation of LAI and fractional cover from small footprint airborne laser scanning data based on gap fraction. *Remote Sensing of Environment*, *104*(1), 50-61.

Parker, G. G. (1995). *Structure and microclimate of forest canopies.* In: Lowman, M.D., Nadkarni, N.M. (Eds.), *Forest Canopies*. Academic Press, San Diego, CA, 73-106.

Pierce, L. L., & Running, S. W. (1988). Rapid estimation of coniferous forest leaf area index using a portable integrating radiometer. *Ecology*, *69*(6), 1762-1767.

Pypker, T. G., Bond, B. J., Link, T. E., Marks, D., & Unsworth, M. H. (2005). The importance of canopy structure in controlling the interception loss of rainfall: examples from a young and an old-growth Douglas-fir forest. *Agricultural and Forest Meteorology*, *130*(1), 113-129.

Richardson, J. J., Moskal, L. M., & Kim, S. H. (2009). Modeling approaches to estimate effective leaf area index from aerial discrete-return LIDAR. *Agricultural and Forest Meteorology*, *149*(6), 1152-1160.

Ryu, Y., Nilson, T., Kobayashi, H., Sonnentag, O., Law, B. E., & Baldocchi, D. D. (2010). On the correct estimation of effective leaf area index: Does it reveal information on clumping effects?. *Agricultural and Forest Meteorology*, *150*(3), 463-472.

Sampson, D. A., & Smith, F. W. (1993). Influence of canopy architecture on light penetration in lodgepole pine (Pinus contorta var. latifolia) forests. *Agricultural and Forest Meteorology*, *64*(1), 63-79.

Savenije, H. H. (2004). The importance of interception and why we should delete the term evapotranspiration from our vocabulary. *Hydrological Processes*, *18*(8), 1507-1511.

Schume, H., Jost, G., & Katzensteiner, K. (2003). Spatio-temporal analysis of the soil water content in a mixed Norway spruce (Picea abies (L.) Karst.)–European beech (Fagus sylvatica L.) stand. *Geoderma*, *112*(3), 273-287.

Seijmonsbergen, A. C. (1992). *Geomorphological evolution of an alpine area and its application to geotechnical and natural hazard appraisal in the NW. Rätikon mountains and S. Walgau (Vorarlberg, Austria)*. PhD dissertation. University of Amsterdam, The Netherlands.

Sinun, W., Meng, W. W., Douglas, I., & Spencer, T. (1992). Throughfall, stemflow, overland flow and throughflow in the Ulu Segama rain forest, Sabah, Malaysia. *Philosophical Transactions of the Royal Society of London B: Biological Sciences*, *335*(1275), 389-395.

Staelens, J., De Schrijver, A., Verheyen, K., & Verhoest, N. E. (2006). Spatial variability and temporal stability of throughfall water under a dominant beech (Fagus sylvatica L.) tree in relationship to canopy cover. *Journal of hydrology*,*330*(3), 651-662.

Swank, W. T. (1968). The influence of rainfall interception on streamflow. In: *Proceedings of the Hydrologic Water Resource Management Conference, 1968 March 28-29, Water Resources Research Institute, Clemson University, 4*, 101-112.

Tabarant, F. (2000). *Apport de la télédétection et de la modélisation à l'étude de la dynamique de production d'un écosystème méditerranéen de chênes verts(Quercus ilex) dans le sud de la France*. PhD dissertation, University of Orsay, Paris, France.

Tromble, J. M. (1983). Interception of rainfall by tarbush. *Journal of Range Management*, *36*(4), 525-526.

US Geological Survey (USGS) (2010). *Digital Aerial Sensor Certification Report for the Microsoft Vexcel UltraCamD, UltraCamX, UltraCamXp and UltraCamXp WA Models*. Received on 13-1-2016 from<<https://calval.cr.usgs.gov/documents/manufacturers_certification/Certification%20Report%20Vexcel%20Ultracam%20Final%20Draft.pdf>>.

Valente, F., David, J. S., & Gash, J. H. C. (1997). Modelling interception loss for two sparse eucalypt and pine forests in central Portugal using reformulated Rutter and Gash analytical models. *Journal of Hydrology*, *190*(1), 141-162.

Van der Meer, F. D., & De Jong, S. M. (2011). *Imaging spectrometry: basic principles and prospective applications*. Dordrecht: Springer Science & Business Media.

Van Dijk, A. I. J. M., & Bruijnzeel, L. A. (2001). Modelling rainfall interception by vegetation of variable density using an adapted analytical model. Part 2. Model validation for a tropical upland mixed cropping system. *Journal of Hydrology*,*247*(3), 239-262.

Van Gardingen, P. R., Jackson, G. E., Hernandez-Daumas, S., Russell, G., & Sharp, L. (1999). Leaf area index estimates obtained for clumped canopies using hemispherical photography. *Agricultural and Forest Meteorology*, *94*(3), 243-257.

Veneklaas, E. J., & Van Ek, R. (1990). Rainfall interception in two tropical montane rain forests, Colombia. *Hydrological processes*, *4*(4), 311-326.

Vose, J. M., Clinton, B. D., Sullivan, N. H., & Bolstad, P. V. (1995). Vertical leaf area distribution, light transmittance, and application of the Beer-Lambert law in four mature hardwood stands in the southern Appalachians. *Canadian Journal of Forest Research*, *25*(6), 1036-1043.

Weiss, M., & Baret, F. (2010). *CAN-EYE V6. 1 User Manual*. Received on 5-9-2015 from <<http://www6.paca.inra.fr/can-eye/Documentation-Publications/Documentation>>

Welles, J. M., & Cohen, S. (1996). Canopy structure measurement by gap fraction analysis using commercial instrumentation. *Journal of Experimental Botany*, *47*(9), 1335-1342.

Williams, D. L. (1991). A comparison of spectral reflectance properties at the needle, branch, and canopy level for selected conifer species. *Remote Sensing of Environment*, *35*(2), 79-93.

Wirth, R., Weber, B., & Ryel, R. J. (2001). Spatial and temporal variability of canopy structure in a tropical moist forest. *Acta Oecologica*, *22*(5), 235-244.

Yu, Q., Gong, P., Clinton, N., Biging, G., Kelly, M., & Schirokauer, D. (2006). Object-based detailed vegetation classification with airborne high spatial resolution remote sensing imagery. *Photogrammetric Engineering & Remote Sensing*, *72*(7), 799-811.

Zhang, Y., Chen, J. M., & Miller, J. R. (2005). Determining digital hemispherical photograph exposure for leaf area index estimation. *Agricultural and Forest Meteorology*, *133*(1), 166-181.

Zhou, L., Pan, G., & Shi, Z. (2010). Methodology comparison for effective LAI retrieving based on digital hemispherical photograph in rice canopy. In: D.Li, Y.Liu & Y.Chen (Eds.), *Computer and Computing Technologies in Agriculture IV* (pp.71-82). Heidelberg: Springer.

Appendix A - Species classification map

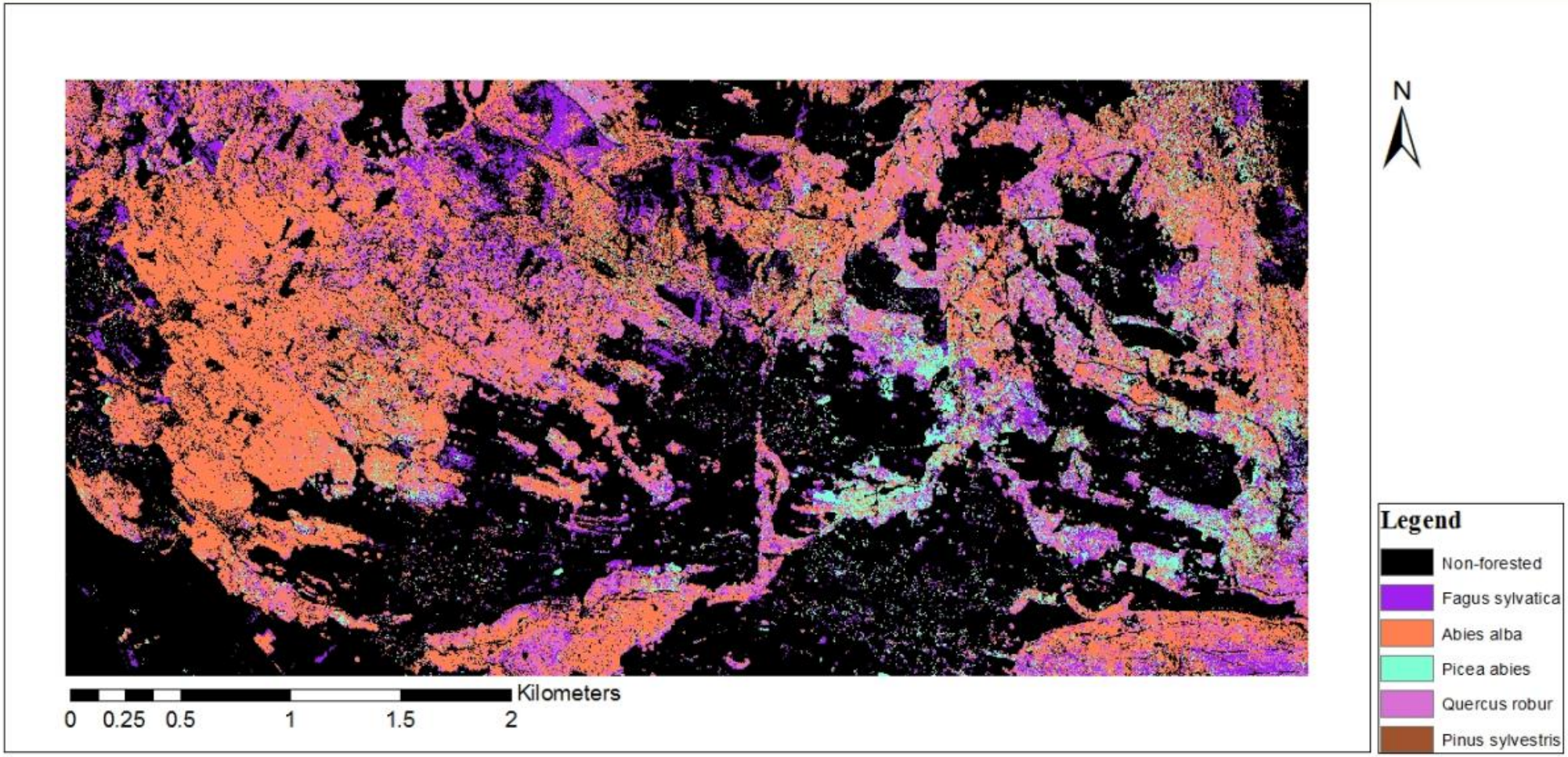

Appendix B - Overall vegetation cover fraction map

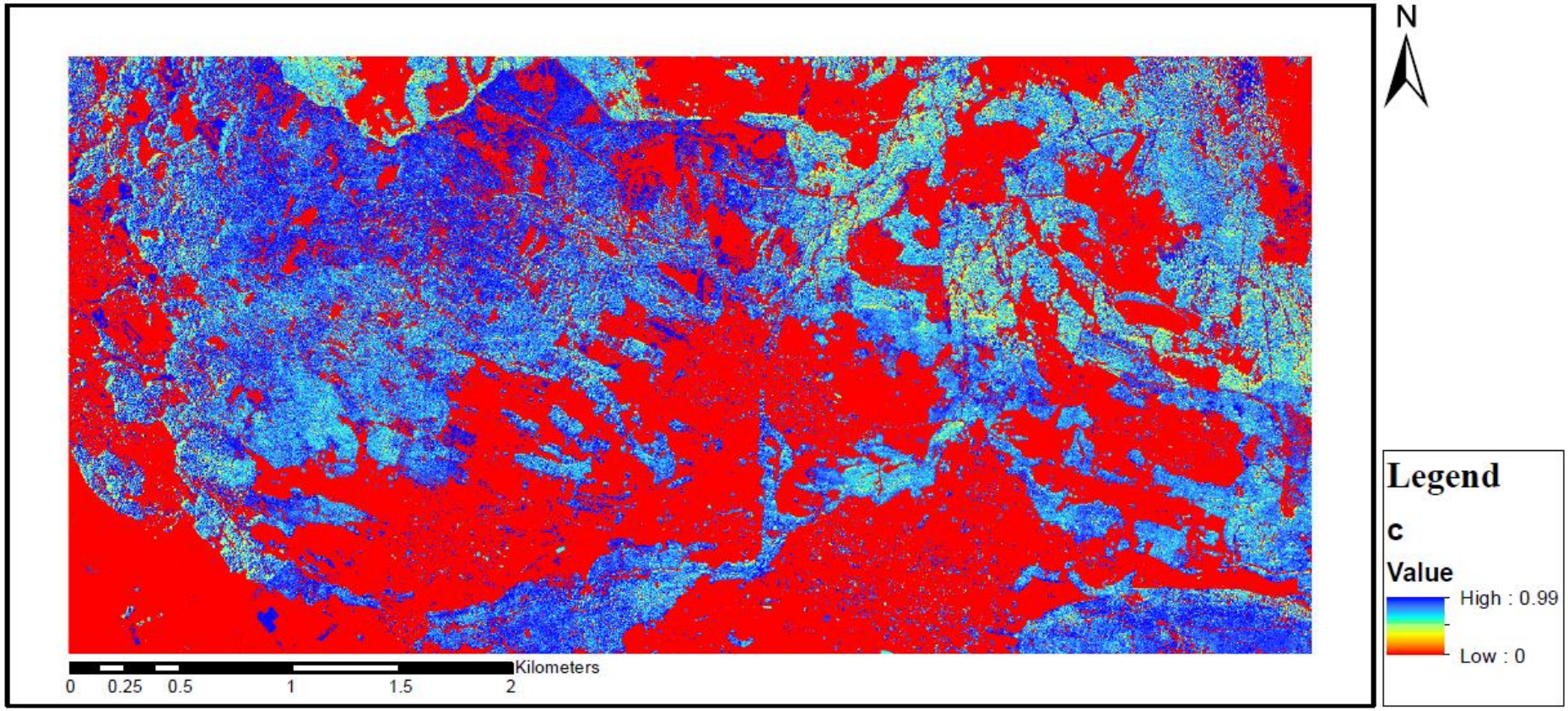

Appendix C - Leaf Area Index map

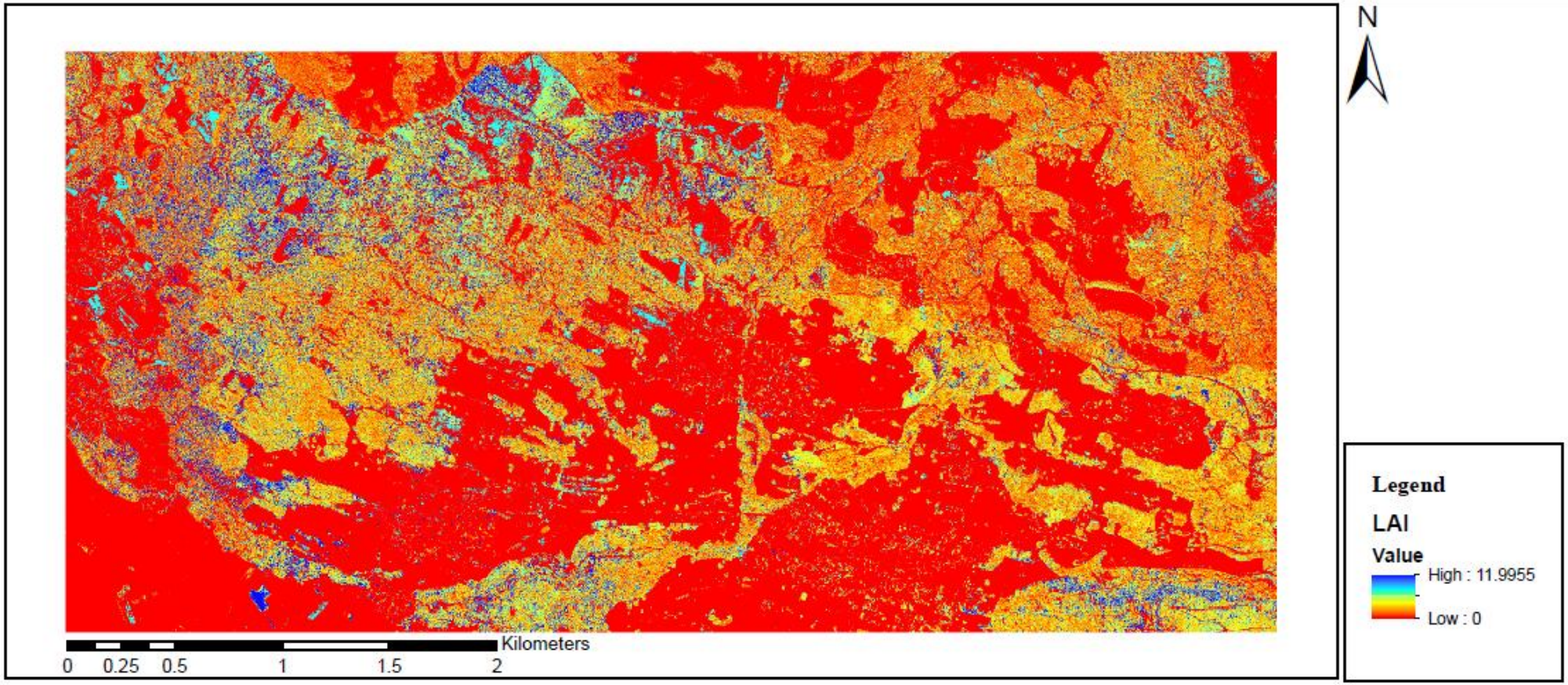

Appendix D - Maximum water storage map

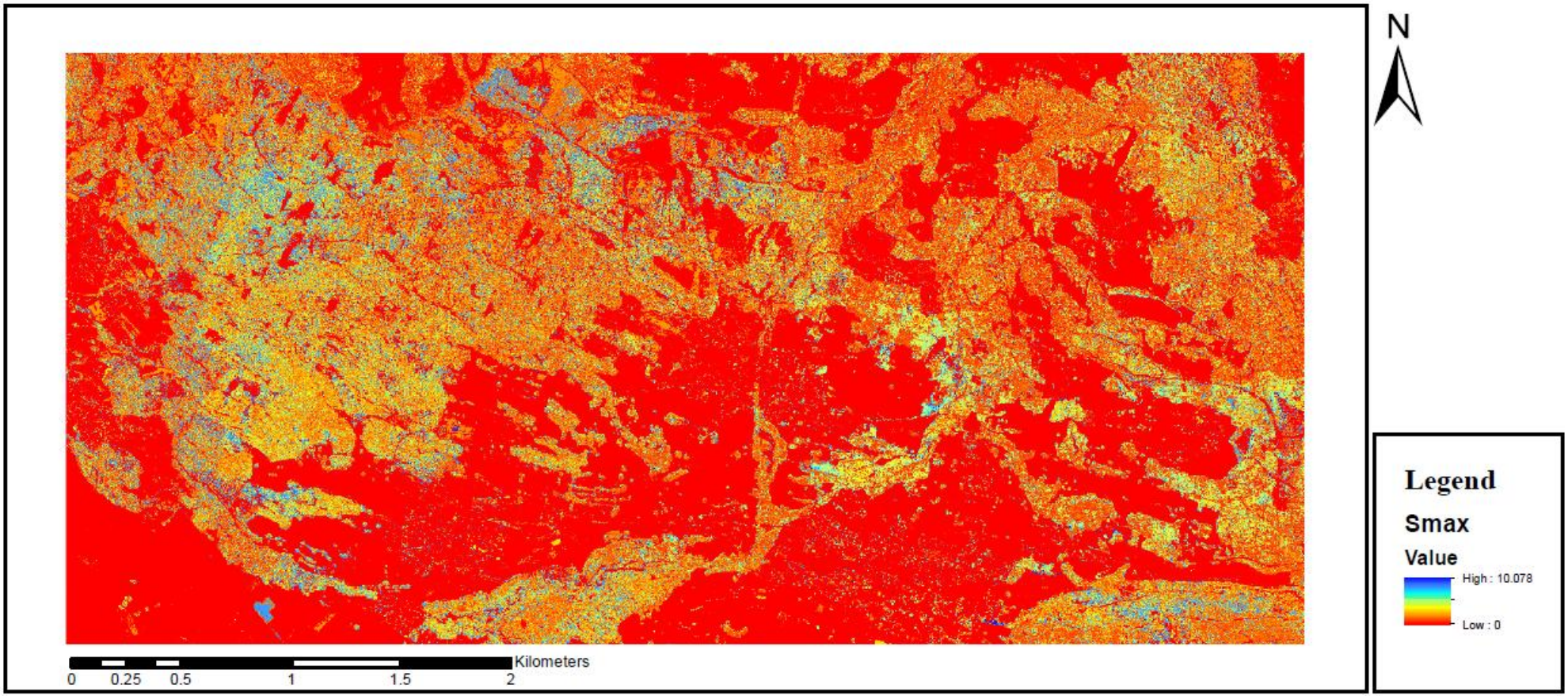

Appendix E - Canopy interception map for P=20.2 mm

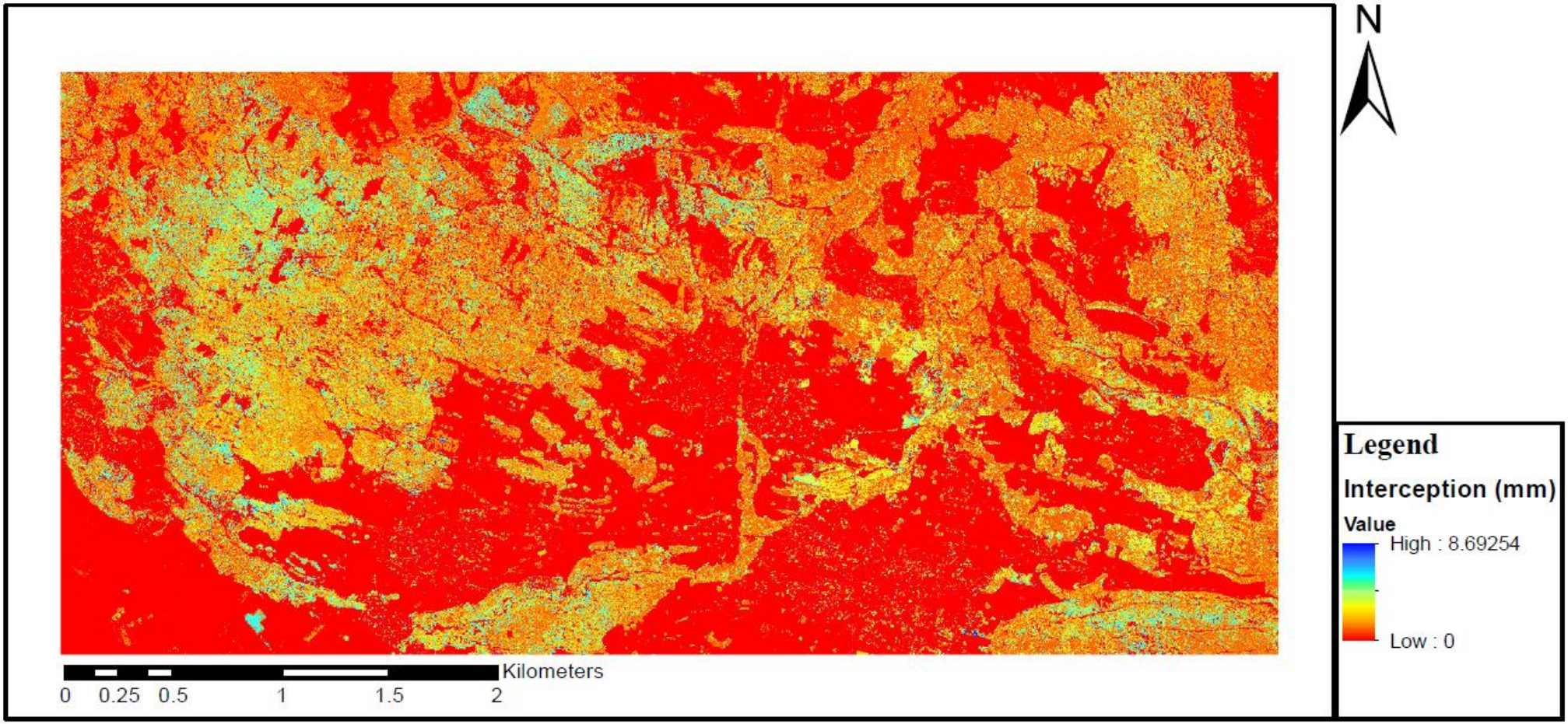

Appendix F - Allometric relations

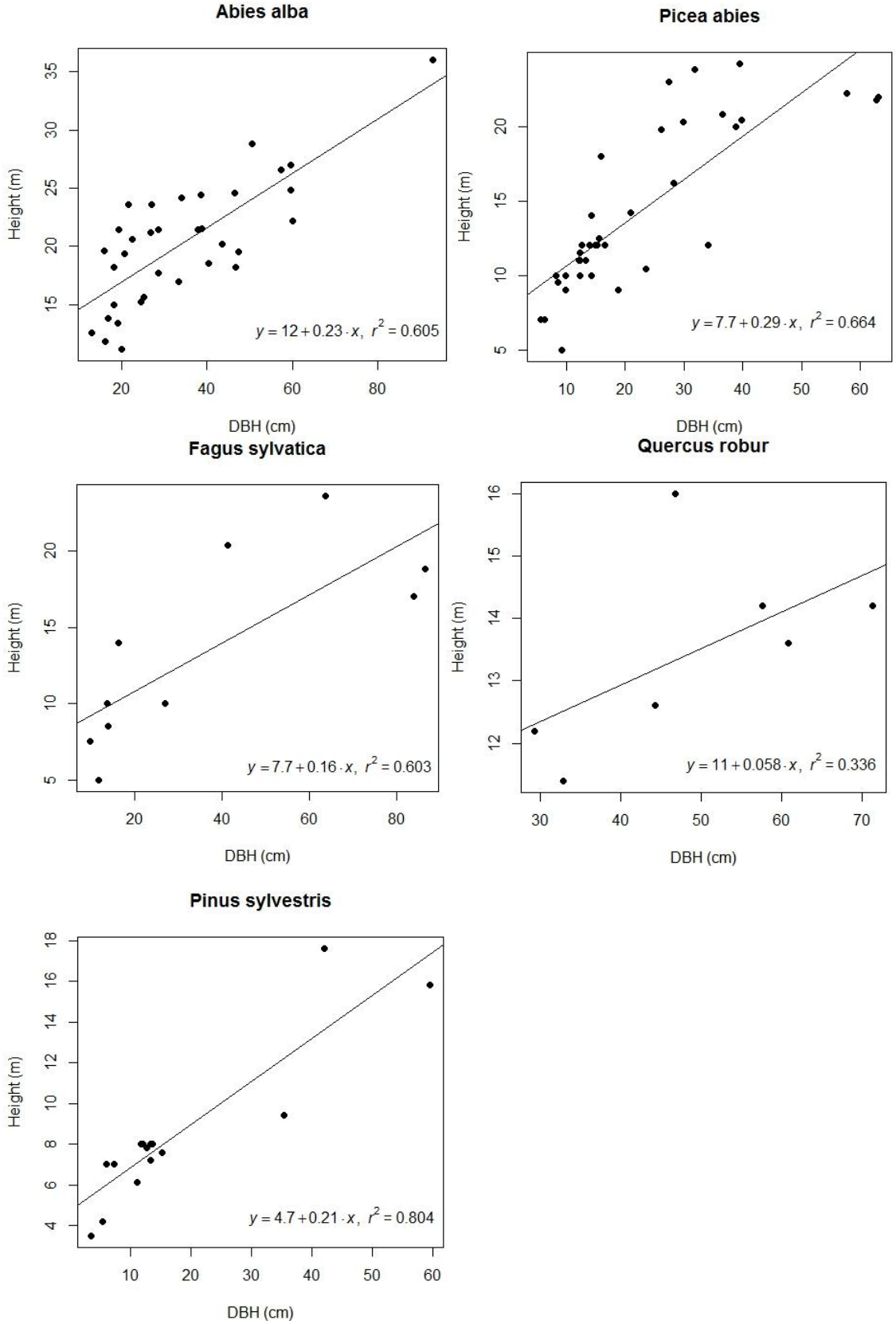

Figure F.1. The species-specific relations between Diameter at Breast Height (DBH) in centimetres and tree height in meters, measured in the plots. The tree heights were estimated using a Nikon Laser 550 AS rangefinder. The DBH is measured using a flexible measuring tape.